Contents TESLA Report 99-20

Interaction Region Layout, Feedback and Background Issues for TESLA

O. Napoly
CEA/Saclay, DAPNIA-SEA, 91191 Gif-sur-Yvette, France

I. Reyzl, N. Tesch
Deutsches Elektronen-Synchrotron, Notkestrasse 85, 22603 Hamburg, Germany

We present the current design of the interaction region for the superconducting linear collider project TESLA. We describe the layout of magnets, separators and collimators which are needed to accommodate a small vertex detector radius in the large aperture appropriate for the head-on collision scheme of TESLA. We then describe the feedback system which will be used to vertically stabilize the beam collisions on a bunch-to-bunch basis down to a fraction of the beam spot size of 5nm. We finally review the various background levels in the detector region, with special attention to the impact of e^+e^- pair and secondary neutron production on the design of the TESLA detector.

1 Introduction

The TESLA superconducting linear collider project [1] aims to produce e^+e^- collisions at 500GeV c.m. energy with luminosity in excess of $10^{34}\text{cm}^{-2}\text{s}^{-1}$. The current parameters of the collider [2] are given in table 1. The design of its interaction region (IR) is mostly driven by three basic ingredients:

- The optics of beam focusing and extraction around the interaction point (IP)
- The diagnostics and correction systems required for reaching and maintaining stable beam operation at the nominal luminosity
- The shielding of nearby components and the masking of the experiment detector from the various accelerator and beam-beam induced background flux

The TESLA final focus optics has some similarities with that of the SLC collider: the beams are focused by high gradient superconducting low-beta quadrupoles with large aperture and they collide at zero crossing angle and are extracted outside of the detector. Indeed, taking advantage of the long RF pulse allowed by the TESLA superconducting linear accelerators, the successive bunches of the TESLA bunch train are equally spaced by about 340ns. It is therefore possible to extract the outgoing beam with a long electrostatic and magnetic separator well before the first parasitic crossing point at about 50m from the IP. However, unlike the SLC, the final doublet quadrupoles are the only magnets common to the incoming and outgoing beam lines. The tuning of both beam lines is therefore coupled in a minimum way.

The luminosity optimization relies on reaching and stabilizing maximum beam overlap and nominal beam sizes at the IP. After the initial tuning of both beam optics separately, this optimization can be divided into three successive levels of tuning procedures:

- The position and angle differences of the colliding bunches at the IP must be cancelled. Thanks to the TESLA pulse structure, the beam separation

can be corrected within a small fraction of the bunch train by a dedicated IP feedback system, as discussed in section 3. This procedure must be repeated on a pulse to pulse basis.

- The transverse beam sizes and linear beam moments (waist-motion, coupling, dispersion, etc..) are measured and tuned. The measurement of the linear beam matrix can be done with a few pulses, using horizontal beam-beam scans for the purely horizontal moments, and luminosity monitoring for the vertical moments and coupling. The correction will be performed by upstream corrector magnets and is believed to remain stable long enough compared to the 5Hz pulse frequency with a slow feedback system steering the beam to a reference orbit.
- Even though the linear optics will be periodically re-tuned, higher order aberrations will slowly develope due to the slow motion of the final focus magnets. The induced degradation of the collider luminosity can be corrected only by beam based re-alignment of the most sensitive elements, like the sextupoles.

Finally, the detector masking and magnet shielding must integrate two specific features of the TESLA design:

- Due to the zero crossing angle, the photon background irradiates the incoming beam line. It is composed of a) high energy beamstrahlung photons, 12GeV energy in average, carrying 300kW average power per side which can damage magnets, and b) widespread synchrotron radiation, 8MeV and 2.1kW average power, produced mostly by the spent beam through the outgoing doublet, which can scatter on close-by elements back to the detector.
- In the current design, the e^- beam must be extracted and transported to the positron target with small beam loss. To accommodate for the capture beam line, the spent beam is bent in the horizontal plane with septum magnets providing the final deflection.

Table 1: Main parameters of the TESLA linear collider.

Parameter	Symbol	Unit	Reference Design
Center of mass energy	E_{cm}	GeV	500
Repetition rate	f_{rep}	Hz	5
Bunch No. per pulse	n_b		2820
Pulse length	t_{pulse}	μs	950
Bunch spacing	t_{bunch}	ns	337
Bunch charge	N	1/e	$2 \cdot 10^{10}$
Horizontal rms beam size at IP	σ_x^*	nm	553
Vertical rms beam size at IP	σ_y^*	nm	5
Vertical divergence at IP	$\sigma_{y'}^*$	μrad	12.3
Vertical Disruption	D_y		33
Luminosity	L_0	$\mathrm{cm}^{-2}\mathrm{s}^{-1}$	$3.1 \cdot 10^{34}$

2 TESLA: Interaction Region Layout

The optics of the beam focusing to the interaction point, depicted in figure 1, is mostly determined by the choice of the free space distance, $l^* = 3$m, from the last

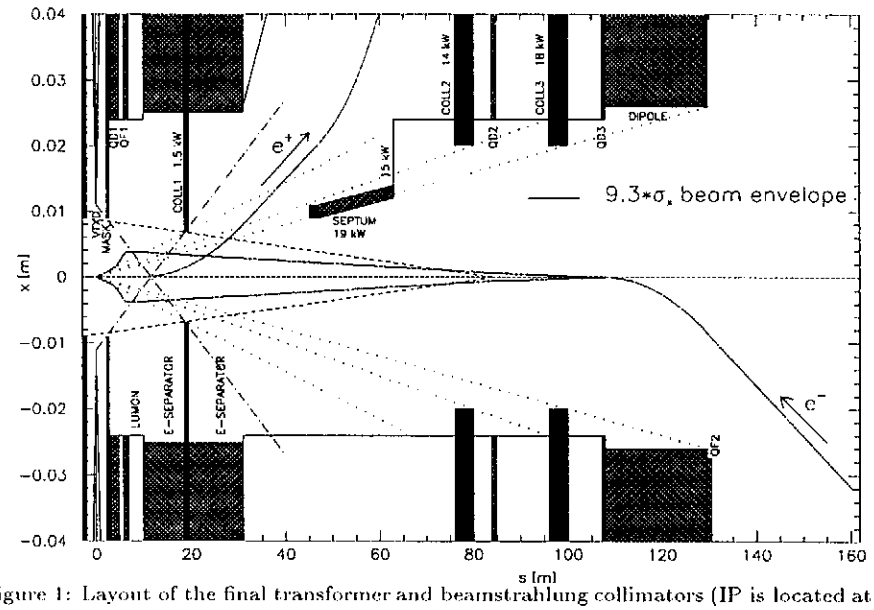

Figure 1: Layout of the final transformer and beamstrahlung collimators (IP is located at s=0).

quadrupole exit to the IP, together with that of the quadrupole magnet superconducting technology. Such quadrupoles[3], combined in a doublet (QF1,QD1), provide the required focusing strength, $G = 250\mathrm{T/m}$, with a large aperture, $R = 24\mathrm{mm}$, necessary to extract the beam as well as the synchrotron radiation background. Their cross section is shown in figure 2(a). These iron-free quadrupoles can stand up to 3T solenoid field with usual NbTi conductors, and over 4T with Nb_3Sn cables. A Tungsten mask with a cylindrical part around the quadrupole cryostat and a 83mrad conical part, as shown in figure 2(b), has been designed [4] to stop the e^+e^- pairs created during the beam-beam interaction and to protect the detector from secondary photons. It also includes an inner cylindrical part to stop the pairs backscattered from the quadrupole face, and to damp the flux of neutrons produced in the collimators outside from the detector. These neutrons are particularly harmful for the vertex detector. Therefore the aperture radius of the inner mask is matched to the radius of the beam pipe at the vertex detector. In figure 2(b), a radius of 18mm was assumed for a 20mm beam pipe radius. In the following study, the mask aperture is reduced to 9mm radius to be able to accommodate a more ambitious design of the vertex detector around a beam pipe radius of 11mm. The role and the performance of the mask will be discussed in more details in section 4.

After the interaction point, the outgoing beam undergoes a first deflection of 8mrad over 20m from an electrostatic separator with $E_x = 48\mathrm{kV/cm}$ across a 5cm gap, combined with a dipole magnet with $B_y = 0.016\mathrm{T}$ in such way that the force acting on the incoming beam, and its polarization, is cancelled. Later, an array of septum magnets over 16m length, provides a second deflection of 2.1mrad to bring

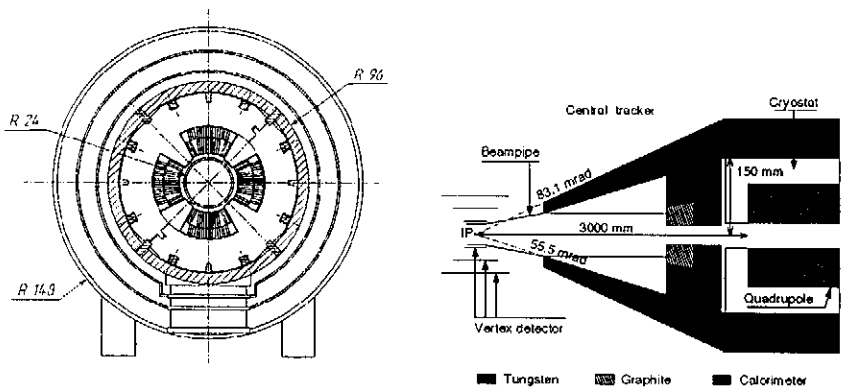

Figure 2: Low-beta SC quadrupole cross section (a) and detector masking system (b).

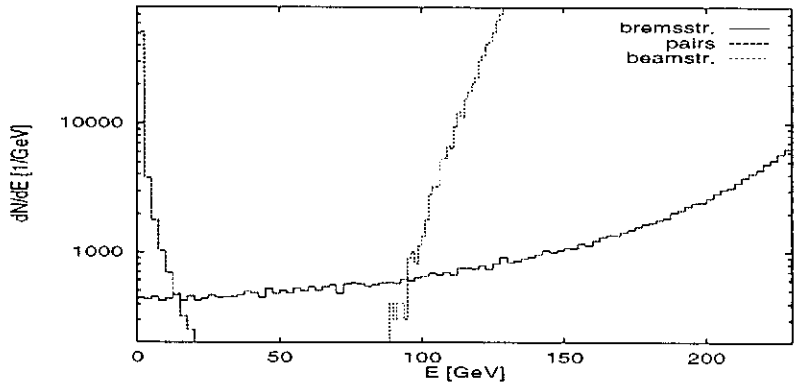

Figure 3: Spectrum of charged particles leaving the IP for a nominal head-on collision.

the spent beam to its capture beam line towards the positron target.

The collimation of the 300kW beamstrahlung photon flux, with about $150 \cdot 34\,\mu\text{rad}^2$ rms divergence from the IP, is done by staged collimators. Figure 1 shows the location of the first four collimators and indicates the amount of beamstrahlung power which they intercept. Collimators 2 and 3 , with a radius of 20mm, are positioned to protect the downstream magnets including the first dipole. The septum is protected by a 2mm thin collimator directly in front of it. The primary role of collimator 1 is to shield the inner part the detector, including the two symmetric inner masks, from the incoming synchrotron radiation generated by the dipole and the quadrupoles up to QD2. Its location is optimized by requiring that, by being close to the IP, its aperture defined by the dashed line of sight from QD2 in figure 1 is large and therefore intercepts as little beamstrahlung power as possible while, by being sufficiently away from the IP, no synchrotron radiation photon can scatter from its edge directly to the beam pipe at the IP, as shown by the dashed-dotted line of sight in figure 1. The optimum location is roughly 19m from the IP. Collimator 1, with an aperture radius of 7mm, thus splits the electrostatic separator in two parts.

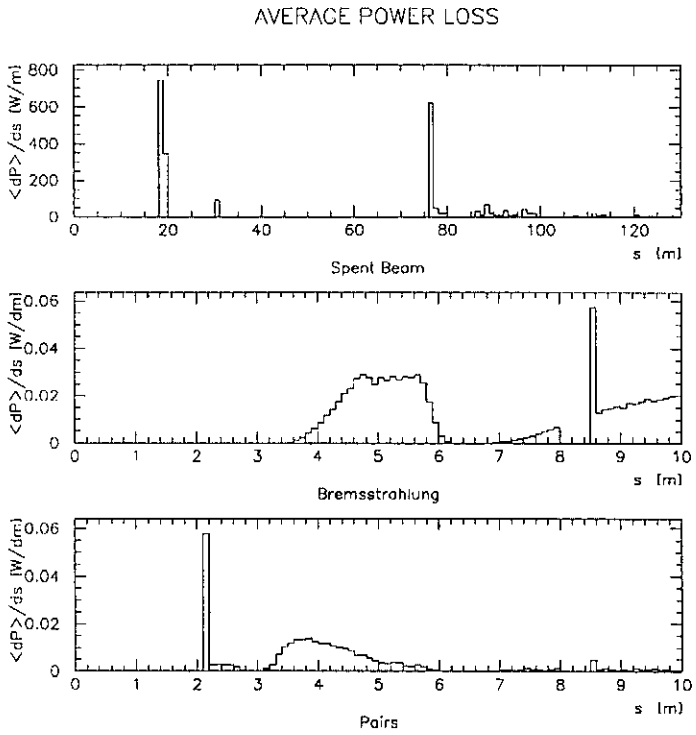

Figure 4: Average power loss along the opposing beam line (the septum collimator is not included in the calculation of the spent beam losses).

This is advantageous because it also intercepts about 1.1kW of spent beam power, as discussed in the next paragraph, and a large fraction of the 2.1kW synchrotron radiation power emitted in the outgoing doublet which would otherwise hit the electrodes of the separator and possibly induce sparking. Except for the quadrupole QF2, figure 1 does not show the location and aperture of the magnets which are centered along the incoming beam line upstream of the dipole. These elements can be shielded from the remaining 240kW of beamstrahlung either by dumping the beamstrahlung flux about 20m after the dipole or, by using flat beam chambers which extend horizontally through the poles of the magnets towards and beyond the beamstrahlung axis in order to clear the photons. In this case the remaining beamstrahlung power can be dumped further down.

To quantify the steady beam losses along the outgoing beam line, we use the distribution of the charged particles after the collision point, assuming ideal beam collisions, obtained from GUINEA_PIG beam-beam simulations[5]. The charged particle spectrum, shown in figure 3, is the superposition of the energy degraded spent beam, at high energy, of the e^+e^- pairs at low energy and, the radiative Bhabha (or *bremsstrahlung*) particles which dominate between roughly 20 and 100GeV. The average deposited power per unit length is shown in figure 4. The pair and radiative Bhabha losses are plotted only along the first 10m after the IP since the spent beam

completely dominates the power loss beyond this point. It is important to note that the power levels along the superconducting doublet cryostat, from 3 to 6.5m, are well below the 4.7W/m LHC tolerance [6]. The spikes in the spent beam power loss correspond to the location of collimators 1 and 2, but the collimator in front of the septum magnet has not been included in the calculation. The spike in the pair power loss is of course at the inner mask face. Finally, the spike in the radiative Bhabha power corresponds to the location of the fast luminosity monitor [7]. It is produced by introducing a gap in the beam pipe from 8 to 8.5m after the IP in order to collect the radiative Bhabhas. Figure 4 shows that higher statistics and less secondary background could be obtained by opening the beam pipe already at 7m from the IP.

3 Feedback System at IP

Due to the large vertical disruption parameter D_y=33, the luminosity is very sensitive to beam separations and crossing angles in the vertical plane, see figure 5. Limiting the maximum luminosity loss per bunch crossing to 10%, two bunches have to interact within a separation of $5\text{Å} = 0.1\,\sigma_y^\star$ and with a crossing angle smaller than 1.2μrad.

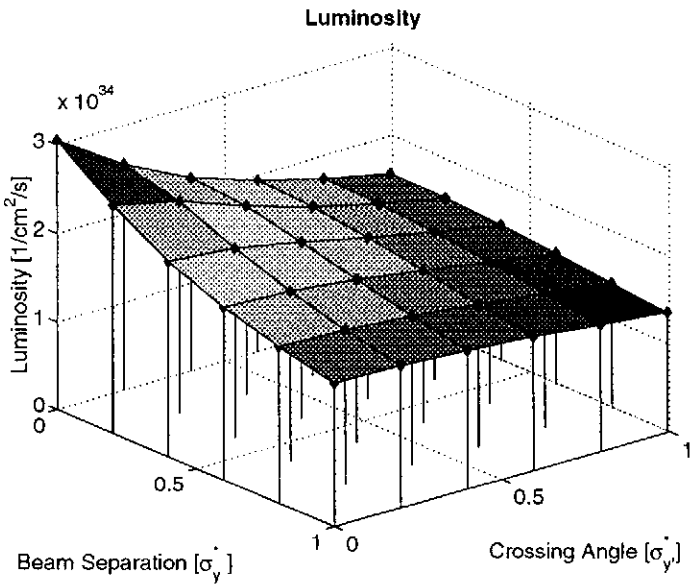

Figure 5: Luminosity as a function of beam separation and crossing angle.

Sources of undesired beam separations and crossing angles are e.g. Lorentz force detuning, wakefield effects and quadrupole vibrations. The displacement of the two opposing final doublet magnets is a major concern, since a stationary final doublet displacement of 5nm = $1\,\sigma_y^\star$ will half the luminosity. Simulations assuming large contributions of human produced noise to the ground motion spectrum [1] predict a $1\,\sigma_y^\star$ beam separation within 1ms, which is roughly the bunch train length. From

pulse to pulse the expected separation might add up to $20\,\sigma_y^\star$ solely due to ground motion effects in the BDS [8].

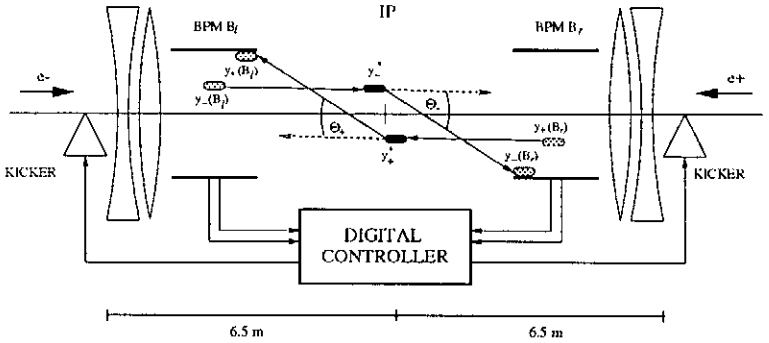

Figure 6: Scheme of the digital feedback system at the IP.

The size and the time scale of the vertical beam separation emphasize the necessity of a feedback system providing a stabilization of the beam interaction at the IP within the bunch train. Due to the large bunch spacing of 337ns a very beneficial correction from one bunch to the second bunch becomes feasible. The design goal is a correction limiting the maximum luminosity loss to 10%. In order to control the other beam angle a further feedback system will remove bunch offsets in the BDS within the bunch train [9].

3.1 IP Feedback Loop

The feedback system at the IP is schematically shown in figure 6. The loop of the digital feedback system (sample frequency 3MHz) is characterized by four steps: detection of bunch separation, estimation of bunch separation, determination of correction kick by a proportional-integral (PI) controller and correction of subsequent bunches by using two fast kickers. The kickers [10], placed on both sides of the IP one meter upstream of the final doublet, allow the coverage of a control range of $\pm 100\,\sigma_y^\star$. The overall processing time of the feedback loop and the signal transmission time in a 50m long cable insert a correction delay of two sample periods. Bunch separations at the IP become detectable by the beam-beam deflection caused by the attraction of the opposite charged bunches [11]. The experienced kick results in measurable position shifts of the outgoing bunches. From the position measurements of the incoming and outgoing bunch of both beams at the two opposing final doublets the size and the sign of the bunch separation can be ascertained.

The separation $\Delta y^\star$ between two bunches is estimated by using a linear model θ^{FB} of the the beam-beam kick, both plotted in figure 7:

$$\theta^{FB}(\Delta y^\star) = -37.27\,\frac{\Delta y^\star}{\sigma_y^\star} \quad [\mu\mathrm{rad}]. \tag{1}$$

The slope of this linear approximation defines how accurately the controller will determine a bunch separation in the nanometer range and by how much large separations will be underestimated.

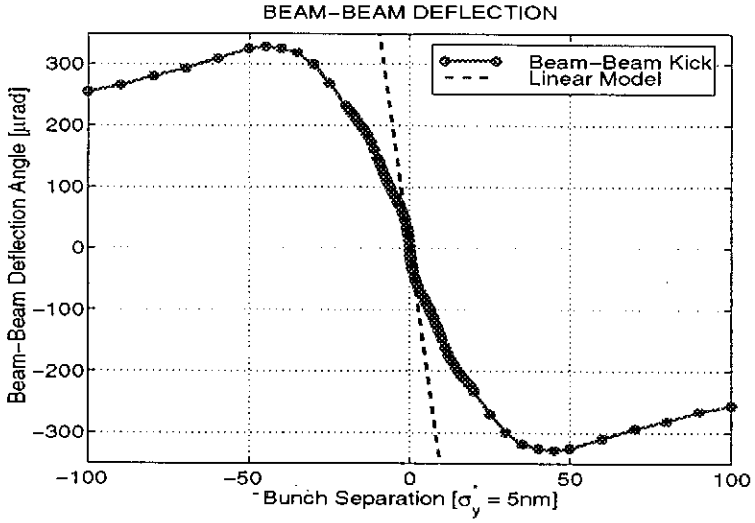

Figure 7: Beam-beam deflection angle θ vs. bunch separation.

3.2 Results

Even though the linear model θ^{FB} used by the feedback system deviates severely from the non-linear beam-beam kick for large separations large stationary offsets are successfully rejected. A constant beam separation of 100 $\sigma_y^\star$ is reduced by 3 orders of magnitude after 80 bunch interactions, emphasizing the robustness of the feedback system to model errors, see figure 8.

During correction the actual vertical separation is continuously underestimated (e.g. $\Delta y^\star = 100\,\sigma_y^\star$ is interpreted as a $7\,\sigma_y^\star$ separation). However, the feedback loop steers subsequent bunches in the right direction decreasing stepwise the occurring offset.

More realistic simulations include the bunch offsets at the linac exit caused by cavity and quadrupole misalignments of 500μm and BPM displacements of 100μm rms. At the IP we further assume a BPM resolution of 5μm (add. noise), quantization errors caused by ADC, a 10% jitter of the beam-beam deflection angle due to bunch charge jitter (mult. noise) and kicker errors of 0.1% (mult. noise). Without the use of a feedback system the luminosity is lowered by 8.4%, whereas a stabilization of the beam interaction by a feedback system allows to achieve 98.6% of the nominal luminosity denoted by L_0.

Assuming an additional stationary beam separation of $50\,\sigma_y^\star$ and $100\,\sigma_y^\star$ caused by ground motion in the BDS and by the displacement of the two final doublets, a luminosity of 95.6% L_0 and 91.8% L_0, respectively, becomes feasible. Limiting the maximum luminosity loss to 10%, the use of the IP feedback system thus relaxes the rms displacement tolerance of pulse-to-pulse jitter of the final doublet magnets to 200nm.

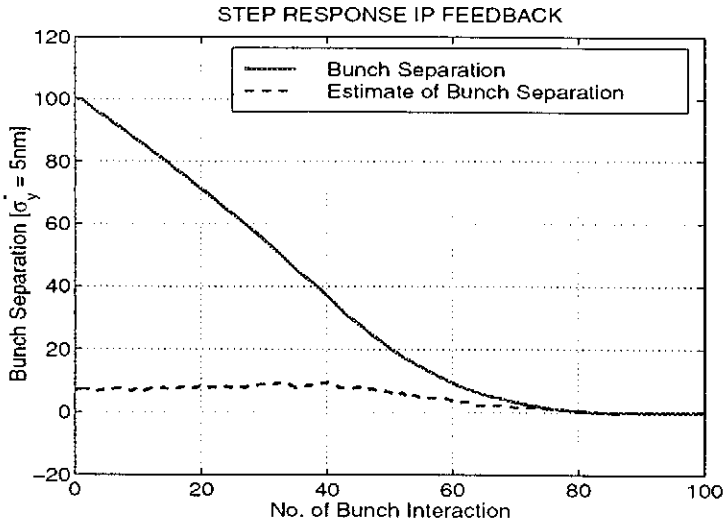

Figure 8: Response to a stationary $100\sigma_y^*$ beam separation.

4 Beam-Beam and Machine Background

4.1 Introduction

The high charge density of the colliding beams produces strong electro-magnetic fields which bend the trajectories of the particles of the oncoming bunch. This focusing effect reduces the effective beam size and enhances the total luminosity. However, at these high energies, this beam-beam interaction also induces an intense emission of hard beamstrahlung photons (in the order of 10^{11} per bunch crossing (BX)) which degrades the energy distribution of the beams during collision. These beamstrahlung photons do not give any direct background signals in the detector, but they can produce a lot of secondary effects, such as pair, charged hadron and neutron production (see figure 9). Beside these beamstrahlung photons, photons can also be created from the elementary process $e^+e^- \rightarrow e^+e^-\gamma$. These photons are no problem as background in the detector, but the remaining electron/positron (radiative Bhabha) whose energy is reduced by the amount of the photon energy can contribute to the neutron background.

On the other hand there are machine related background sources: Muons can be created in electro-magnetic beam-nucleon interactions in the beam delivery system. These muons can reach the IP and can cause an intolerable background in the detector. The collimation system of TESLA is done such that no direct synchrotron radiation can reach the detector. But the edge- and backscattering of the synchrotron radiation of the incoming and outgoing beam from elements of the collimation system can be a potential source of background. Finally beam-gas interactions can contribute to the background in the detector. All background sources are described in more detail elsewhere [1,4].

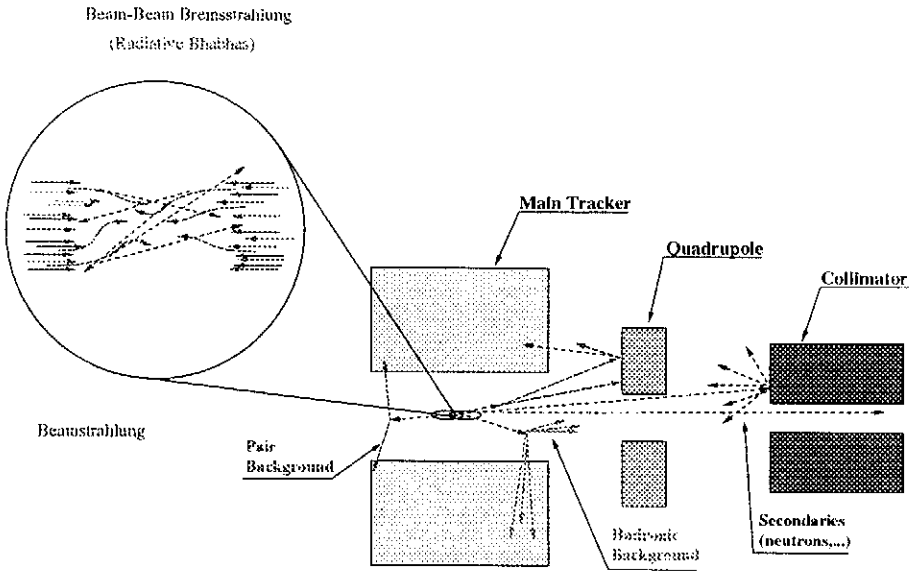

Figure 9: Illustration of different background sources.

4.2 Beamstrahlung

The two bunches focus each other at the interaction point due to the high charge density of beams which leads to strong electro-magnetic fields. This effect is called the 'pinch effect'. Since the particle trajectories are bent due to the pinch effect they emit a radiation called beamstrahlung (BS). This leads to an energy loss of the electrons and positrons. For TESLA the photons have energies in the range of a few GeV. The center of mass energy for the collisions will hence vary more than expected from the energy spread of the incoming beams and the initial state radiation. Since the pinch effect reduces the effective beam cross sections the luminosity is enhanced compared to the nominal one. To study the BS different Monte Carlo programs were developed to simulate the pinch effect and the secondary physical processes. Three generators (GUINEA_PIG [4], CAIN 2.1b [12], LINCOL 1.0 [13]) were used and their results are compared in table 2.

The beamstrahlung photons produced by the program GUINEA_PIG were used as an input to a GEANT3 [14] based simulation of the TESLA detector and beam line called BRAHMS [15]. There were no direct hits from BS in any detector element with the present collimation system found.

4.3 Pairs

One of the main background sources in the detector is the production of electron-positron pairs via coherent or incoherent processes in the beam-beam interaction. The coherent ones can be neglected in the TESLA case. Three main processes contribute to the incoherent production of electron-positron pairs:

Table 2: Comparison of beamstrahlung results from different generators.

	GUINEA_PIG	CAIN 2.1b	LINCOL 1.0
δE_{beam} [GeV]	6.92	6.80	7.62
δE_{beam} [%]	2.77	2.72	3.05
N_γ per electron	1.65	1.62	1.70
$\overline{E_\gamma}$ [GeV]	4.19	4.20	4.48
N_γ / BX [10^{10}]	6.60	6.48	6.80
E_γ / BX [J]	44.3	43.5	48.8
P_γ [MW]	0.63	0.61	0.69

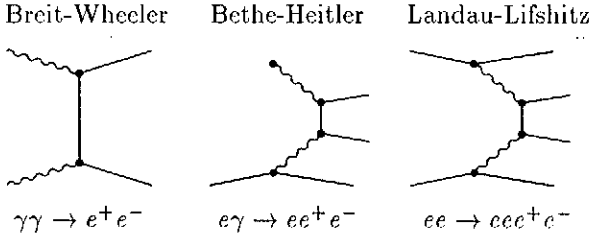

The Bethe-Heitler and Landau-Lifshitz processes can be calculated using the equivalent photon approximation, in which the electron (and positron) are replaced by a spectrum of photons. For the Breit-Wheeler process the two colliding photons are real, where for the Bethe-Heitler one photon is real and one virtual and for the Landau-Lifshitz processes both photons are virtual.

Table 3: Comparison of pair production results from different generators.

	GUINEA_PIG	CAIN 2.1b	LINCOL 1.0
N_{pairs} / BX [10^3]	120	82	73
E_{pairs} / BX [10^3GeV]	295	193	175
$p_t > 20$MeV			
$\theta > 150$mrad			
N_{pairs} / BX	50	32	46
E_{pairs} / BX [GeV]	6.61	3.60	5.95

Again the above described three Monte Carlo programs were used and their results for pair production are compared in table 3. The pair particles produced by the GUINEA_PIG program were tracked through the TESLA detector simulation BRAHMS (see figure 10) and the following results were found: For a radius between 0.9cm and 5.4cm at the front side of the mask the deposited energy is 27.3TeV per BX (26.4TeV per BX) for a main magnetic field of 3T (4T). For radii greater than 5.4cm (corresponding to an angle larger than 23.5mrad) the energy deposition is 6GeV per BX for 3T and 4T. Therefore instrumentation of the front side of the mask seems to be possible for at least angles down to 23.5mrad to measure physics

based events. In the vertex detector of the current design of the TESLA detector there were 690 charged hits per BX in the first layer (at 1.2cm) found for the 3T case and 334 for the 4T case. The number of photons created from pair particles entering the TPC was found to be 1350 per BX (3T) with an average energy of 1.7MeV and 1200 per BX (4T) with an average energy of 1.6MeV. The conclusion can be made that the numbers of photons from the pair background in the TPC is non-critical and that both discussed vertex detector pixel designs (APS,CCD) even for a 1cm beam pipe and 3T main magnetic field are feasible.

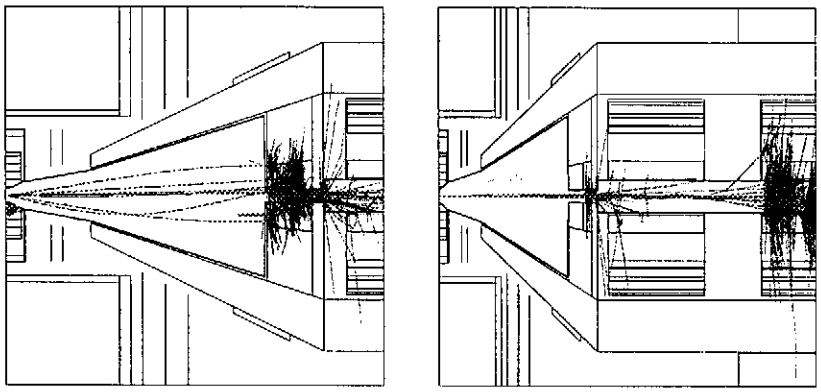

Figure 10: Some pair particles showering at the front side of the mask and some radiative Bhabhas showering at the final quadrupole doublet (from TESLA detector simulation BRAHMS).

4.4 Radiative Bhabhas

Another process that produces low energy particles is the elementary process $e^+e^- \rightarrow e^+e^-\gamma$. Here the beam particle emits a hard photon in the field of a single oncoming particle (beam-beam bremsstrahlung). The calculation is done using the equivalent photon approximation. The photon escapes through the beam pipe, while the remnant beam particle contributes to the background. These low energy beam electrons/positrons, called radiative Bhabhas (RB), will be dumped in the final quadrupole doublet and will produce electro-magnetic showers and neutrons in the material of the quadrupoles (see figure 10). The consequences are that some of the electro-magnetic shower particles (photons/electrons) as well as the produced neutrons from inside the quadrupoles can reach the detector.

As a generator the GUINEA_PIG program was used. Applying a cut of 100GeV (to select only these particles which will hit the final quadrupole doublet) gives a total number of radiative Bhabhas of $N_{tot} = 4.9 \cdot 10^4$ per BX with a total energy of $E_{tot} = 2.6 \cdot 10^6$GeV per BX.

Again these particles were tracked through the TESLA detector simulation with the result that all electrons/positrons with an energy E >90GeV pass the final quadrupole doublet. In the first layer of the vertex detector (at 1.2cm) 2 charged hits per BX were found for a main magnetic field of 3T and the number of photons entering the TPC was found to be 3 per BX for 3T. In conclusion the amount of direct background hits in the detector from radiative Bhabhas is small.

4.5 Neutrons

Neutrons are produced via photo-nuclear reactions from electro-magnetic shower bremsstrahlung photons. The dominant neutron production via the giant photo-nuclear resonance mechanism is in the photon energy range between 10-30MeV. Therefore any γ,e^+,e^- hitting a beam line element and creating electro-magnetic showers is a potential source of neutrons.

The simulation of neutron production was done using the program FLUKA98[16]. This program can handle the production and transport of neutrons from thermal energies up to 20TeV for primary and secondary particles. It can simulate the low energy neutron production down to 0.4eV in ENEA multigroups. The low energy neutron transport is done via photon and fission neutron generation and the photo and electro-hadron/nuclear production is using the vector meson dominance model. The geometry of the TESLA detector and beam line in FLUKA98 can be seen in figure 11.

The total number of neutrons produced from beamstrahlung photons is $N_{tot} = 2.5 \cdot 10^{10}$ per BX with a total energy $E_{tot} = 2.4 \cdot 10^8$GeV per BX. For the pairs these numbers are $N_{tot} = 4.9 \cdot 10^4$ per BX with $E_{tot} = 262$GeV per BX and for the radiative Bhabhas $N_{tot} = 2.7 \cdot 10^5$ per BX with $E_{tot} = 2.1 \cdot 10^3$GeV per BX (see figure 11 for production location of neutrons from different sources). The numbers of neutrons entering some individual detectors could be found in table 4 for the vertex detector, TPC and electro-magnetic calorimeter (barrel/endcap). The fluxes for the vertex detector are given as total fluxes for all neutrons and in brackets as fluxes normalized to 1MeV neutrons, weighted due to the silicon bulk damage by total non ionizing energy loss (NIEL).

In conclusion one can say that the fluxes at the vertex detector are in the order of $4 \cdot 10^8$ n/cm^2/year and that means both options (APS,CCD) seem to be possible in terms of the neutron background. The total numbers of neutrons of about 6000 per BX in the TPC and of about 4000 (8000) per BX in the ECAL barrel (endcap) seem to be a non critical amount of neutron background.

Table 4: Results from FLUKA98 for neutrons entering individual detector parts.

	VDET n (1MeV n) /cm^2/year	TPC n/BX (E_{tot}[GeV])	ECAL(b) n/BX (E_{tot}[GeV])	ECAL(ec) n/BX (E_{tot}[GeV])
n from BS	$2.8 \cdot 10^8$	2400	1800	2100
	$(0.5 \cdot 10^8)$	(5.1)	(4.3)	(3.7)
n from Pairs	$< 0.5 \cdot 10^8$	3200	2300	3100
	$(0.0 \cdot 10^8)$	(8.6)	(6.1)	(13.5)
n from RB	$< 0.5 \cdot 10^8$	44	31	2300
	$(0.0 \cdot 10^8)$	(0.002)	(0.001)	(13.5)
total	$< 3.8 \cdot 10^8$	5600	4100	7500
	$(0.5 \cdot 10^8)$	(13.7)	(10.4)	(30.7)

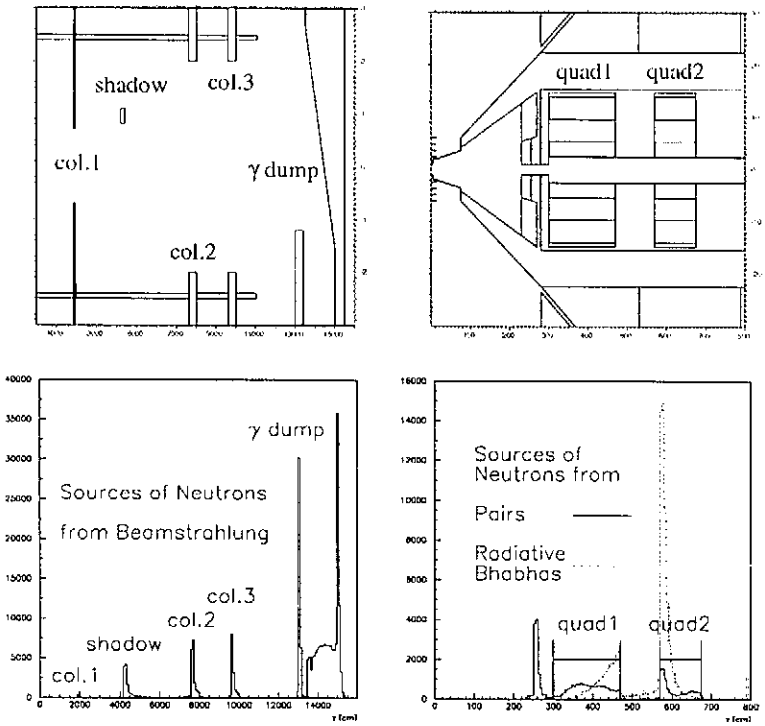

Figure 11: FLUKA98 geometry for TESLA beam line and mask region. Production location of neutrons for different sources: beamstrahlung, pairs and radiative Bhabhas.

4.6 Hadrons

An additional source of background is the production of hadrons by two colliding photons ($\gamma\gamma \to hadrons$). In this process the photons fluctuate into hadrons with the same quantum numbers and with a certain probability a photon can interact hadronically as a vector meson (mainly as ρ^0). Three cases are to be distinguished for the production of hadrons by two colliding photons:

direct once resolved double resolved

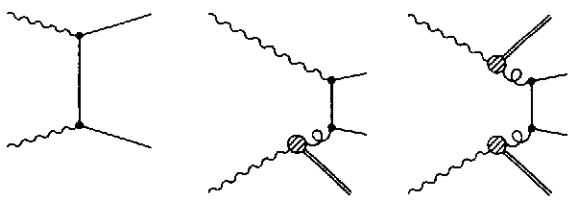

$\gamma\gamma \to jj$ $\gamma\gamma \to j_s jj$ $\gamma\gamma \to j_s j_s jj$

The simulation of $\gamma\gamma \to hadrons$ was done such as the photons were taken from the beamstrahlung simulation (GUINEA_PIG) and the $\gamma\gamma$ interaction was simulated by HERWIG 5.9, with multiparton interaction on and HERWIG default parameters except for the HERA DIS tuning[17]. In table 5 the results can be found for the three different cases. Only about $2 \cdot 10^{-2}$ events per BX are expected.

Table 5: Results for hadron production at TESLA.

type	events /BX [10^{-2}]	mult.	charg. mult.	E_{tot} /BX [GeV]
direct	0.53	15.2	8.5	0.25
single res.	0.40	30.5	15.7	0.32
double res.	1.12	44.7	22.2	1.50
all	2.05	34.3	17.4	2.07

From the TESLA detector simulation BRAHMS the following numbers for some detector parts were derived: In the first layer (2./3./4./5.) of the vertex detector 3.39 (0.66/0.42/0.29/0.23) $\cdot 10^{-3}$ charged hits per cm^2 per BX were found for a main magnetic field of 3T. In the TPC 8.5 gammas per BX with a mean energy of 2.6MeV and 0.7 charged particles per BX were found. The energy flow into the ECAL barrel is 2.0GeV per BX and 4.0GeV per BX for the endcap. In conclusion one can say that the hadron background found in the detector is small.

4.7 Muons

In e^+e^- linear colliders muons are produced in electro-magnetic beam-nucleon interactions in the beam delivery system due to partial beam loss in beam line elements. They can contribute an intolerable background in the detector. When electrons or positrons strike beam line elements muons are produced by a variety of mechanisms: Bethe-Heitler process ($\gamma Z \rightarrow \mu^+\mu^- Z$, dominant), photo production of π ($\gamma Z \rightarrow \pi(\rightarrow \mu\nu) + X$) and direct annihilation ($e^+e^- \rightarrow \mu^+\mu^-$). Even the muons produced far away from the IP can traverse the tunnel parallel to the beam line and reach the detector. Therefore in the simulation all beam line elements of the beam delivery system (-1200m $\rightarrow$ IP) and the tunnel are included. The dominant channel $\gamma Z \rightarrow \mu^+\mu^- Z$ was investigated in the current simulation studies. The detector is defined as a disk of radius 4.5m at the IP. A detailed description of this study can be found elsewhere[18]. The results of this simulation can be seen in figure 12, where the number of lost electrons to produce one muon in the detector is plotted as a function of the source location.

One finds in average about $2.5 \cdot 10^4$ lost electrons to get one muon in the detector. Additional magnetized iron toroids (2 toroids a 9m at 866m/1060m from the IP) help to reduce the muon background by a factor 10. Introducing an iron doughnut (120m iron at 800m) helps to reduce the muon background by a factor of 1000.

4.8 Backscattered Synchrotron Radiation

Synchrotron radiation will be produced by the incoming beam in the magnetic field of the last bending magnet. Also in the field of the final quadrupole doublet synchrotron radiation will be produced by the incoming and outgoing beam. The collimation system is made such that no direct synchrotron radiation hits any part of the detector, but backscattered photons can be a potential background source for

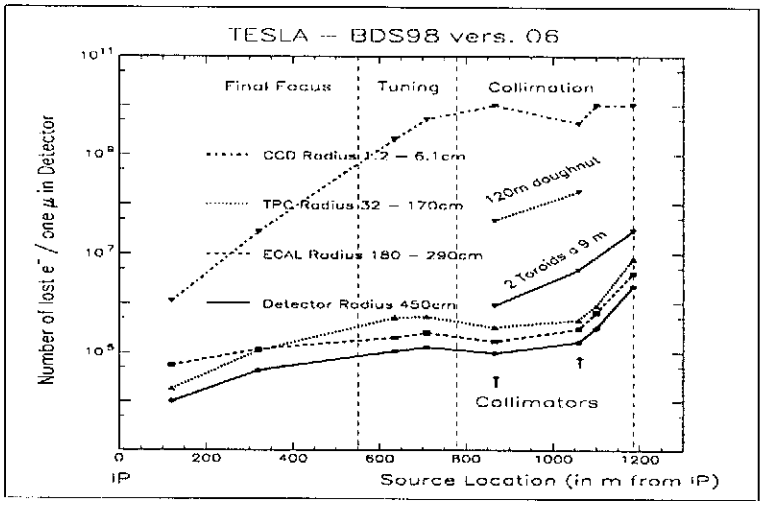

Figure 12: Number of lost electrons needed to produce one muon in the detector as a function of the source location.

the detector. The main source for backscattered synchrotron radiation is the first collimator at 19m from the IP. Table 6 shows the amount of synchrotron radiation hitting the first collimator. The calculation of backscattered synchrotron radiation into the detector takes into account the energy spectrum, the angular distribution and the albedo of the collimator material, resulting in 60 photons per cm^2 per BX in the vertex detector with energies of E_γ <1MeV. Approximately no backscattered photons reach the TPC and the ECAL.

Table 6: Synchrotron radiation hitting the first collimator.

source	N_γ	scattering	N_γ (scat. at col.1)
inc. beam/last bend	$5 \cdot 10^{10}$	edge + back	10^8/BX
inc. beam/final quad	$2 \cdot 10^{11}$	back	10^8/BX
out. beam/final quad	$4 \cdot 10^{11}$	back	$2 \cdot 10^{11}$/BX

4.9 Beam-Gas

The main sources of rest gas inside the beam pipe are on the one hand the material outgasing, which is a global effect and on the other hand the synchrotron radiation, which is a local effect. For the simulation of the beam-gas interaction it was assumed to have as rest gas CO with a pressure of $p = 5 \cdot 10^{-9}$mbar. Tracking was performed through the last 600m of the beam line, including quadrupoles, collimators, mask and a beam pipe of 1cm radius.

As result there were $3 \cdot 10^{-3}$ electrons per bunch crossing found which are leaving the beam pipe near the IP with an energy of about $E \approx 0.2 \cdot E_{beam}$. So the background expected in the detector from beam-gas interactions will be very small.

Table 7: Summary of all background sources at TESLA for beamstrahlung (BS), pairs (PA), radiative Bhabhas (RB), neutrons (N), hadrons (HA), muons (MU), backscattered synchrotron radiation (BSR) and beam-gas interaction (BGI).

Source	N_{tot} /BX	E_{tot} GeV/BX	VDET hits/cm^2/BX	TPC /BX	EC(b) /BX	EC(ec) /BX
BS	$6.6 \cdot 10^{10}$	$2.8 \cdot 10^{11}$	-	-	-	-
PA	$1.2 \cdot 10^{5}$	$3.0 \cdot 10^{5}$	690 (1.layer, 3T)	1350γ (3T)	-	-
RB	$4.9 \cdot 10^{4}$	$2.6 \cdot 10^{6}$	2 (1.layer, 3T)	3γ (3T)	-	-
N/BS	$2.5 \cdot 10^{10}$	$2.4 \cdot 10^{8}$	$2.8 \cdot 10^{8}$ n/cm^2/year	2400	1800	2100
N/PA	$4.9 \cdot 10^{4}$	262	$< 0.5 \cdot 10^{8}$ n/cm^2/year	3200	2300	3100
N/RB	$2.7 \cdot 10^{5}$	$2.1 \cdot 10^{3}$	$< 0.5 \cdot 10^{8}$ n/cm^2/year	44	31	2300
HA	$2.1 \cdot 10^{-2}$ events	2.1	$3.4 \cdot 10^{-3}$ (1.layer, 3T)	8.5γ (3T) 0.7char.(3T)	2.0GeV	4.0GeV
MU	$2.5 \cdot 10^{4}$ N_e/μ		$2.5 \cdot 10^{7}$ N_e/μ	$1 \cdot 10^{5}$ N_e/μ	$5 \cdot 10^{4}$ N_e/μ	$5 \cdot 10^{3}$ N_e/μ
BSR	$2.0 \cdot 10^{11}$	$2.0 \cdot 10^{8}$	60γ/cm^2/BX	-	-	-
BGI	$3 \cdot 10^{-3}$	0.15	-	-	-	-

5 Conclusion

The IR picture described in this paper offers a coherent solution to the beam transport and detector protection assuming the most demanding beam and detector conditions considered up to now for TESLA, namely:

- High luminosity $L = 3 \cdot 10^{34}\text{cm}^{-2}\text{s}^{-1}$, corresponding to the beam parameters with high beam-beam disruption
- Capture and transport of the e^- spent beam after collision, towards the positron source target
- Vertex detector of about 1cm radius, combined with high solenoid field of 4T

While the global design of the collider design is under progress, these options are still being discussed. If some of them are eventually removed, we believe that the IR design can only be easier and its layout simpler. The 800GeV center of mass energy option of TESLA has also been studied and does not change qualitatively the conclusions reached in this study. Vertical stabilization of the beam collision by a bunch-to-bunch feedback system is necessary and feasible. Limiting the maximum luminosity loss due to bunch separations to less than 10% relaxes the rms tolerance of the final doublet pulse-to-pulse displacements to 200nm.

The comparison of the generation of beamstrahlung and pairs between three different simulation programs showed reasonable agreement. From the background from pairs and radiative Bhabhas found in the detector one can conclude that the instrumentation of the mask will be possible down to 23.5mrad and that for the vertex detector both pixel options (APS,CCD) are possible. The neutron flux in the vertex detector was found to be moderate, so that also from this side both options (APS,CCD) seem to be feasible. The neutron background in the TPC and the ECAL seem to be handleable. Only small amounts of background signals from hadrons, backscattered synchrotron radiation and beam-gas interaction were found

in the detector (see table 7). So we can state that with the present knowledge of background at TESLA we foresee no problems for the presently studied detector design.

Acknowledgments

We are particularly grateful to D. Schulte and A. Drozhdin for their valuable help and advice while this study was being done. We also would like to thank R. Brinkmann, R.-D. Kohaupt, S. Schreiber and N. Walker for many useful discussions. Finally we thank A. Ferrari for providing us with the program FLUKA98.

References

1. R. Brinkmann, G. Materlik, J. Rossbach, A. Wagner, *Conceptual Design of a 500 GeV e^+e^- Linear Collider with integrated X-ray Laser Facility*, DESY 1997-048, 1997; ECFA 1997-182, 1997
2. R. Brinkmann, *High Luminosity with TESLA 500*, DESY, TESLA 97-13, 1997
3. J.M. Rifflet et al., *Cryogenic and Mechanical Measurements of the first two LHC lattice Quadrupole Prototypes*, EPAC94 Conf., London, UK, 1994
4. D. Schulte, *Study of Electromagnetic and Hadronic Background in the Interaction Region of the TESLA Collider*, Ph.D. Theses 1997, DESY TESLA 97-08, 1997
5. D. Schulte, *Beam-Beam Simulation with GUINEA_PIG*, ICAP Conf., Monterey, CA., U.S.A., 1998; CERN/PS 99-014, 1999
6. A. Devred, private communication
7. O. Napoly, D. Schulte, *Luminosity Monitor Options for TESLA*, LINAC98 Conf., Chicago, U.S.A., 1998
8. N. Walker, private communication, DESY 1999
9. I. Reyzl, *Fast Feedback Systems for Orbit correction in the TESLA Linear Collider*, IEEE Conf. Proc. of the PAC 99, New York, U.S.A., 1999
10. J. Rümmler, *Feedback Kickers in the DESY Rings*, IEEE Conf. Proc. of the EPAC 94, London, England, 1994
11. P. Bambade, R. Erickson, *Beam-Beam Deflection as an Interaction Point Diagnostic for the SLC*, SLAC-PUB 3979, 1986
12. K. Yokoya, T. Tauchi et al., *Program CAIN 2.1b*, http://www-acc-theory.kek.jp/members/cain
13. V. Telnov, *Program LINCOL 1.0*, private communication
14. *GEANT, Detector Description and Simulation Tool*, CERN Geneva, Switzerland 1993
15. T. Behnke, G. Blair et al., *BRAHMS - Version 1.02, A Monte Carlo for a Detector at a 500/800 GeV Linear Collider*, http://www.ifh.de/linear_collider
16. A. Fasso, A. Ferrari, J. Ranft, P. Sala et al., *Program FLUKA98*, manual and code available from authors
17. N. Brook et al., *Tuning Monte Carlo Event Generators to HERA Data*, UCL/HEP 96-05, 1996
18. M. Sachwitz, H.J. Schreiber, *Muon Background in a 500GeV TESLA Linear Collider*, DESY, TESLA 94-27, 1994

INSTRUMENTATION AT THE INTERACTION REGION OF A LINEAR e^+e^- COLLIDER.

S. SCHREIBER
Deutsches Elektronen-Synchrotron, 22603 Hamburg, Germany

A future TeV-scale linear e^+e^- collider will operate with ambitious beam parameters at the interaction region in order to achieve the luminosity required for physics experiments. It will be essential to measure and monitor relevant beam parameters close to the interaction point in order to obtain and maintain high luminosity. This report gives an overview on the beam parameters to be measured and discusses examples of proposals for the required instrumentation and their implementation in the interaction region.

1 Introduction

A stable operation of a TeV-scale linear e^+e^- collider with the highest luminosity possible will be a key requirement for the success of the physics program. To obtain a luminosity in the $10^{34}\,cm^{-2}s^{-1}$ range, ambitious beam parameters like low emittance and nanometer scale beam sizes at the interaction point (IP) have been proposed[1,2]. Beam parameters will be measured at various places in the linac and in the beam delivery system (BDS). However, due to the large demagnification ($\times$ 200 to 300), it is hardly possible to accurately predict the beam parameters at the IP from the measurements in the BDS alone. Instrumentation in the interaction region (IR) is therefore required to achieve optimal beam quality. But it has to be considered as well, that place constraints close to the vertex detector require the instruments being as compact and least invasive as possible.

2 Overview on Beam Parameters

Table 1 gives an overview on relevant beam parameters to be measured after acceleration, either up- or downstreams the IR, most of them in the BDS. This report concentrates on those parameters to be measured in the interaction region. The table also gives typical values and resolutions required.

To summarize and ordering the items by priority, the following parameters have to be considered to be measured in the IR: relative luminosity (beam aberrations), vertical beam spot size, beam position, vibration and drift of the final quadrupoles, horizontal beam spot size, and beam induced particle background. Other parameters of importance like vertical and horizontal emittance, energy, energy spread, and beam polarization will be measured in the

Table 1: Relevant beam parameters to be measured. It is indicated, if the measurement should be in the interaction region (IR) or if a measurement elsewhere is sufficient: in the beam delivery system (BDS), up- or downstreams the IR. Typical values and resolution required are given. The exact numbers depend on the specific collider proposal.

parameter	measured at	value	resolution
vertical spot size	IR	3 to 5 nm	few %
horizontal spot size	IR	200 to 500 nm	few %
bunch length	BDS	90 to 400 μm	few %
emittance	BDS	0.01 to 0.1 μm (vert.)	few %
energy	ds IR	250 to 500 GeV	10^{-4}
energy spread	ds IR	10^{-3}	1 %
beam position	IR	-	1 to 5 μm
beam jitter and drift	IR	-	10 nm
vibration	IR	-	10 nm
beam polarization	us or ds IR	60 (e^+) to 80 % (e^-)	1 %
beam phase stability	BDS	2° (X-band)	-
rel. luminosity	IR	-	1 %
luminosity spectrum	IR	-	1 %
background	IR	-	-
bunch charge	BDS	0.6 to 3.5 nC	few %

beam delivery system or downstreams of the IP. They are not discussed in this report.

Highest priority is given to the measurement of the relative luminosity and the vertical beam size. A luminosity monitor allows to correct for beam aberrations and to optimize collision parameters. The optimization of the vertical beam size is of utmost importance, since it limits the achievable luminosity and is the most difficult one to achieve. Once collision is established, beam position measurements are required to stabilize the collision with feedback systems. Beam position monitors (BPM) will also serve to measure beam jitter and drifts of the beam in respect to the final quadrupoles.

Some of these measurements will be performed from bunch to bunch, eg. the beam position for a feedback system. For most other monitors, it is sufficient to measure from train to train, since the beam should be sufficiently stable during one bunch train[2]. Measurements of vibrations of critical elements in the IR like the final quadrupoles are helpful to justify this assumption. However, especially in cases, where a feedback system to maintain collision is not easily realizable, vibration measurements together with a stabilization of the final quadrupoles are essential.[3]

Most of the resolutions required for the various measurements are not very ambitious and can be realized by known techniques. One exception is the measurement of vertical beam spot sizes below 10 nm. Resolutions required for the BPMs are in the range of 1 to 5 μm. This has already been achieved with present technologies. However, for vibration and drift measurements, the BPM resolution should approach the vertical spot size.

In the following, two examples of instrumentation in the interaction region are discussed: the luminosity monitor and the beam size measurement.

3 Luminosity Monitor

Stabilization of the colliding beams is achieved with a feedback system based on the minimization of beam-beam kicks.[4] This system requires BPMs between the mask and the final quadrupole and kickers to steer the beam.

The beam-beam deflection scan method is a useful tool to tune the beam while in collision. It has little impact on the integrated luminosity and has been used successfully eg. at the SLC.[5] However, in the case of large vertical disruption this method fails to deconvolute the vertical spot size from the measurement. In this case, a combination of horizontal beam-beam deflection scans to measure the horizontal aberration and luminosity scans for the vertical aberration seams to be a feasible tool to tune the beam.[6] The luminosity measurement can be realized by two methods: (a) measuring the low angle radiative Bhabhas (bremsstrahlung) in a calorimeter situated several meters away from the IP, and (b) measuring the e^+e^--pair background in a calorimeter integrated into the inner part of the mask (Fig. 4(a)). In method (a), radiative Bhabhas will be measured background free in the energy gap between the background from pairs and from off momentum electrons (positrons) which have radiated beamstrahlung. The Bhabhas are being deflected by the final quadrupoles, and can be detected 8.5 m from the IP in a calorimeter around the beam pipe (TESLA case). 25 bunch crossings are sufficient to reduce the statistical error below 1 % allowing a complete scan within a bunch train.[6]

To correct linear aberrations which effect the vertical beam size, different scans have been proposed. Two examples of waist shift scans are shown in Fig. 1. A resolution of 1 % per measured point during the scan leads to a luminosity optimization with a precision expected to be better than 10^{-3}. For method (b), a calorimeter will be installed in the inner part of the mask to measure the energy of the beam induced pair background. The total energy deposited below 20 mrad is in the order of 30 TeV per bunch crossing[8] and poses thus a challenge for the detector construction. The advantage of this method compared to (a) is, that the relative resolution of 1 % can be reached

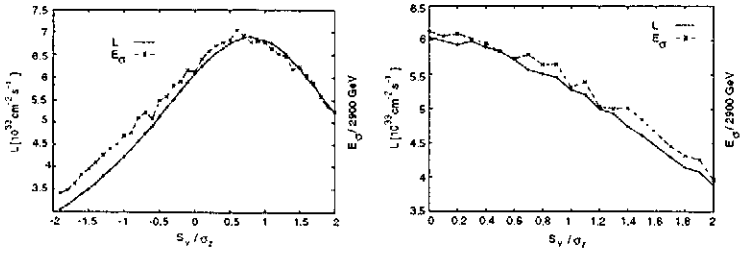

Figure 1: Comparison of luminosity L and energy E_σ deposited by the e^+e^- pairs in the inner part of the mask: (left) the two vertical waists are symmetrically shifted against each other along the beam axis by S_y with respect to the collision point; (right) two coinciding vertical waists are shifted together with respect to the collision point. (From TESLA CDR[7])

already with one bunch crossing.

4 Beam Size Monitor

A difficult task will be the measurement of the vertical beam spot size at the IP, which is in all linear collider proposals less than 10 nm. At the Final Focus Test Beam (FFTB), a method based on a laser interferometer[9] has been developed and successfully used to measure spot sizes down to 60 nm.[10] For the measurement of larger spot sizes in the range of 500 nm to some μm, a laser wire has been tested SLD.[11] Other methods have been proposed to measure nm spot sizes, eg. by measuring the angular distribution of the pair background.[12] Here, the vertical spot size is indirectly obtained by measuring the horizontal spot size and the aspect ratio. However, scanning methods are model dependent and cannot deconvolute the contributions from the opposite beam and thus leave the uncertainty which beam has to be corrected.

4.1 Laser Interferometer

A laser beam with good coherence is split into two beams, which are combined to generate an interference pattern at the location of the electron beam (Fig. 2). The spacing between the fringes is a few times larger than the beam size to be measured. The electron beam is swept over the fringe pattern. The rate of Compton scattered photons is measured as a function of the beam sweep. The result is a modulated signal, with the modulation depth M being a direct measure of the beam size (Fig. 3a):

$$M(\sigma) = K|\cos\theta|e^{-2(\frac{2\pi}{\lambda}\sin\frac{\theta}{2})^2\sigma^2}$$

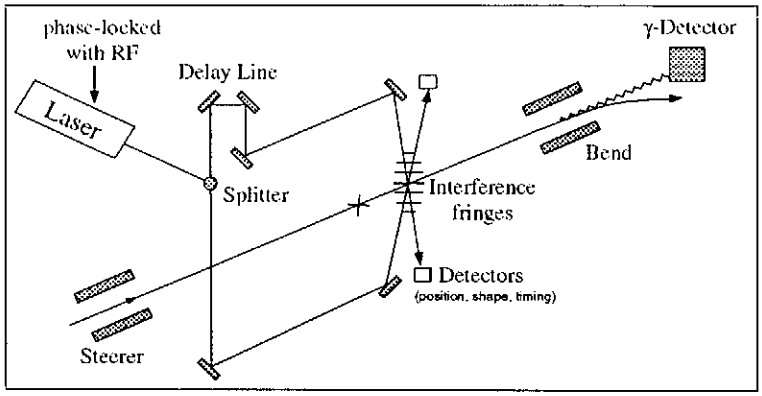

Figure 2: Principal components of the laser beam size monitor. The electron or positron beam is swept over the fringe pattern generated by the two arms of the split laser beam. The Compton scattered photons are measured as a function of the sweep.

If the angle θ between the laser arms is chooses to be close to 180°, the modulation depends only on the laser wavelength λ. Since the wavelength of a laser beam is precisely known, this method provides a direct measure of the absolute spot size. However, systematic corrections indicated by the factor K have to be applied. It has been shown, that these corrections can be kept below 10 %.[10]

The range of spot sizes accessible by the laser interferometer is determined by the wavelength of the laser and the resolvable modulation depth (Fig. 3b). With a careful setup and sufficient statistics, a modulation measurement of up to 0.95 and down to 0.05 should be possible. Assuming a standard laser source like Nd:YLF, a wavelength of 262 nm would allow to measure in the range from 51 nm down to 6.7 nm, a wavelength of 209 nm from 41 nm down to 5.3 nm, with the latter being extremely difficult to realize. This would just include the vertical beam size of TESLA, but not of NLC or JLC.

The electron position jitter in respect to the laser fringes has to be smaller than the bunch size to be measured. Therefore, the spot size measurement should be accompanied by a beam jitter measurement eg. with a high resolution BPM. The usefulness of the combination of spot size measurement and beam position and jitter measurement at the IP and the image point of the final focus system has been shown during the FFTB runs. A C-band cavity BPM has been developed, which reached a remarkable resolution of 25 nm.[13]

In order to be useful in a train by train beam correction scheme, one complete spot size measurement will be done within a pulse train. This is especially appealing in the TESLA case, where a large number of almost 3000

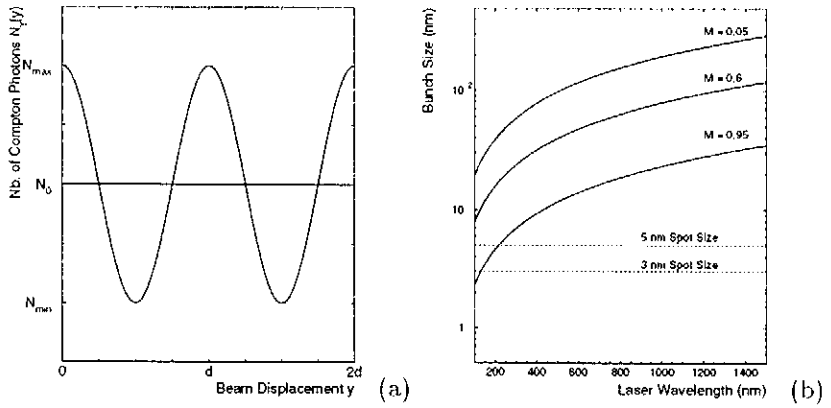

Figure 3: (a) Modulated Compton rate as a function of the beam displacement, d is the fringe distance. (b) Dynamic range of the laser beam size monitor as a function of laser wavelength. The lines indicate the measurable bunch sizes for a modulation depth M of 0.95, 0.6, and 0.05 ($\theta = 175°$).

bunches per train can be used. A suitable laser for this would be a mode-locked system synchronized to the electron bunch train. The expected Compton rate is large enough to collect sufficient statistics: $N_\gamma = 600 \cdot N_e/10^{10} \cdot P/\mathrm{MW}$. The number of electrons per pulse is typically $N_e = 10^{10}$, a laser beam power of $P = 1\,\mathrm{MW}$ is obtained by modern ps laser systems. One point of concern is the possible damage of optical elements by higher power UV laser radiation. This has to be carefully take into account for in the design of the monitor.

For stability reasons, the last optical elements, the mirror and focusing optics are preferably to be mounted onto the detector mask, which itself is a heavy rigid structure (Fig. 4(b)). Incorporating most of the optics into the mask reduces additional dead material inside the detector to a minimum. The laser and beam steering devices will be outside the detector. The mask will not extend down to the interaction point. Therefore, the electron or positron beam waist has to be shifted for the measurement away from the IP by 800 mm.

The horizontal spot sizes of all collider proposals are larger than the accessible range of the laser beam size monitor. A thinkable solution would be to reduce the angle θ between the split laser beams from 180° to the mask cone angle of $2 \times 83\,\mathrm{mrad}$. This would allow a measurement of spot sizes in the range between $150\,\mu\mathrm{m}$ and $1.2\,\mu\mathrm{m}$ ($\lambda = 523\,\mathrm{nm}$) with the cost of larger systematic uncertainties.

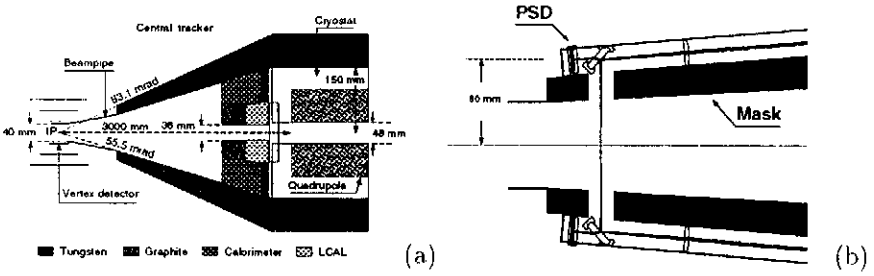

Figure 4: (a) Mask layout to suppress the background from pair creation. Indicated is the proposed position of the luminosity calorimeter (LCAL) and the BPM between the mask and the quadrupole cryostat. (b) Possible mechanical implementation of the optics for the laser beam size monitor into the mask. Indicating are position sensitive devices (PSD).

4.2 Laser Wire

The electron beam is swept over a strongly focused laser beam. The Compton signal is unfolded with the shape of the laser beam to extract the electron beam size. In order to reduce potential systematic errors due to uncertainties in the laser beam shape, the laser spot must be smaller than the beam size. To estimate the achievable spot size, the geometrical constraints at the IP have to be considered. For a suitable location of the laser wire in the IR, the last focusing mirror would have distance to the beam line of about $l = 100\,\mathrm{mm}$. Allowing a laser spot diameter at the mirror of $D = 30\,\mathrm{mm}$, the smallest achievable waist would be $w = 2\sigma_r = \frac{\lambda}{\pi} / \arctan(\frac{D}{2l}) \approx 2\lambda$. Choosing $\lambda = 262\,\mathrm{nm}$, a laser spot size down to $\sigma_r = 280\,\mathrm{nm}$ could in principle be realized under perfect conditions. This would just work for TESLA, but is too large for the other proposals. For this reason, a laser wire to measure the horizontal spot size at the IP seams not to be feasible.

5 Conclusion

Including beam instrumentation into the interaction region is difficult but necessary: a calorimeter for relative luminosity measurements inside the inner part of the mask, a laser interferometer to measure the vertical beam size, and beam position monitors for an orbit feedback system and for vibration measurements. Commissioning of the final focus system will certainly be done before the particle physics detector is in place. This will allow for testing of the proposed instrumentation, but leaves also room for additional equipment, eg. to measure beam induced backgrounds. Once the final focus is commis-

sioned and the detector is in place, a minimum of instrumentation will still be required to verify, maintain, and optimize the beam quality.

Acknowledgments

The author would like to thank in particular T. Shintake for his help and the material he provided for this workshop, O. Napoly, R. Brinkmann, I. Reyzl, T. Behnke, and N. Tesch for many fruitful discussions.

References

1. N. Phinney, "The Next Linear Collider", these proceedings;
   S. Iwata, "The Japanese Linear Collider Project" these proceedings.
2. R. Brinkmann, "The TESLA Linear Collider", these proceedings.
3. T. Markiewicz, "NLC Interaction Region Issues and IP Layout", these proceedings.
4. R. D. Kohaupt, I. Reyzl, "Fast Feedback System for Orbit Corrections in the TESLA Linear Collider", Proc. of the 1999 Part. Acc. Conf., New York City, March 29th - April 2nd, 1999, p. 1171;
   L. Hendrickson et al., "Feedback Systems for Linear Colliders", Proc. of the 1999 Part. Acc. Conf., New York City, March 29th - April 2nd, 1999, p. 338.
5. P. Emma, L.J. Hendrickson, P. Raimondi, F. Zimmermann, "Limitations of Interaction-Point Spot-Size Tuning at the SLC", SLAC-Pub-7509 (1997).
6. O. Napoly, D. Schulte, "Luminosity Monitor Studies for TESLA", TESLA 97-17, Nov. 1997.
7. R. Brinkmann, G. Materlik, J. Rossbach, A. Wagner (ed.), "Conceptual Design of a 500 GeV e^+e^- Linear Collider with Integrated X-ray Laser Facility", DESY 97-048 and ECFA 97-181, 1997.
8. O. Napoly, I. Reyzl, N. Tesch, "Interaction Region Layout, Feedback and Background Issues for TESLA", these proceedings.
9. T. Shintake, "Proposal of a nanometer beam size monitor for e^+e^- linear colliders", Nucl. Instrum. and Meth. A311 (1992) 453.
10. V. Balakin et al., "Focusing of Submicron Beams for TeV-scale Linear e^+e^- Colliders", Phys. Rev. Lett., 74 (1995) 2479.
11. D. Arnett et al., "SLC/SLD Laserwire", Proc. of the 6th Intern. Workshop on Linear Colliders, March 27–31, 1995, Tsukuba, Japan, KEK proceedings 95-5, p. 1525.
12. T. Tauchi, K.Yokoya, "Nanometer beam-size measurement during collisions at linear colliders", Physical Review E 51 (1995), 6119-6126.
13. T. Shintake, "Development of Nanometer Resolution RF-BPMs", KEK-PREPRINT-98-188, Nov. 1998.

HIGH-ENERGY BREMSSTRAHLUNG AT TESLA

K. PIOTRZKOWSKI [a]
DESY, Notkestraße 85, D-22607 Hamburg, Germany
and
Institute of Nuclear Physics, Kawiory 26A, PL-30055 Kraków, Poland

It is argued that the properties of high-energy bremsstrahlung in e^+e^- collisions make it a very attractive tool for measurements of the luminosity and beam properties at the linear colliders. More detailed considerations including a suggestion of a possible detector realization are presented assuming the design parameters of TESLA.

1 Introduction

A good control of beam properties in the interaction regions of the future linear colliders as well as precise luminosity measurements are big experimental challenges. Due to a strong beam focusing and resulting extremally small lateral beam sizes there will be very strong electromagnetic fields acting on all charged particles in the interaction region. It will result in a number of phenomena as an additional beam focusing (beam-pitching) or in strong coherent radiation called *beamstrahlung*, for example. On the other hand, the neutral particles as for example photons which are not are affected by these fields are ideal probes of the properties of the colliding beams. In particular, the bremsstrahlung photons emitted in e^+e^- collisions and carring energies close to the beam energy have an unique feature of accurate mapping of the angular distributions and (longitudinal) polarization of beam particles. Moreover, since the high-energy bremsstrahlung cross-section is sizable and well understood therefore the bremsstrahlung rate could be a precise and direct measure of the collider luminosity.

2 High-energy e^+e^- bremsstrahlung

The main characteristics of the high-energy bremsstrahlung are extremaly small momentum transfers between colliding electrons and positrons. The typical momentum transfers $\Delta_{||}$ along the collision axis for photon energy E_γ are near the minimum value,

$$\Delta_{||}^{min} \approx \frac{M_e^2}{2E_{beam}} \frac{y}{1-y},$$

[a] krzysztof.piotrzkowski@desy.de.

where M_e is the electron mass, E_{beam} is the beam energy and $y = E_\gamma / E_{beam}$. For example, if $E_{beam} = 250$ GeV and $y = 0.5$ then $\Delta_{||}^{min} \approx 0.13$ eV which corresponds (via the uncertainty principle) to micron-size distances. The lateral momentum transfers are also very small and may in principle reach zero. In other words, the high-energy bremsstrahlung occurs over finite macroscopic distances $l_f = h/\Delta_{||}$ called the photon *formation lengths*. If during the photon formation the incident electron (or positron) is scattered or deflected by an angle bigger than about M_e/E_{beam} then bremsstrahlung is suppressed.

According to Chen & Klein [1], the relevant suppression at the considered future linear colliders may occur only due to deflection of a radiating electron (or positron) by the coherent electromagnetic field of the opposite beam. The scaling variable for this effect is $\Upsilon = \frac{5}{6} r_e^2 E_{beam} N / \alpha \sigma_z (\sigma_x + \sigma_y)$, where r_e is the classical electron radius, N is the number of particles in a bunch and $\vec{\sigma}$ is the nominal Gaussian beam width at the interaction point (IP). If $\Upsilon \ll 1$ then bremsstrahlung is suppressed [1] for $y \lesssim \frac{2\Upsilon}{1+2\Upsilon}$.

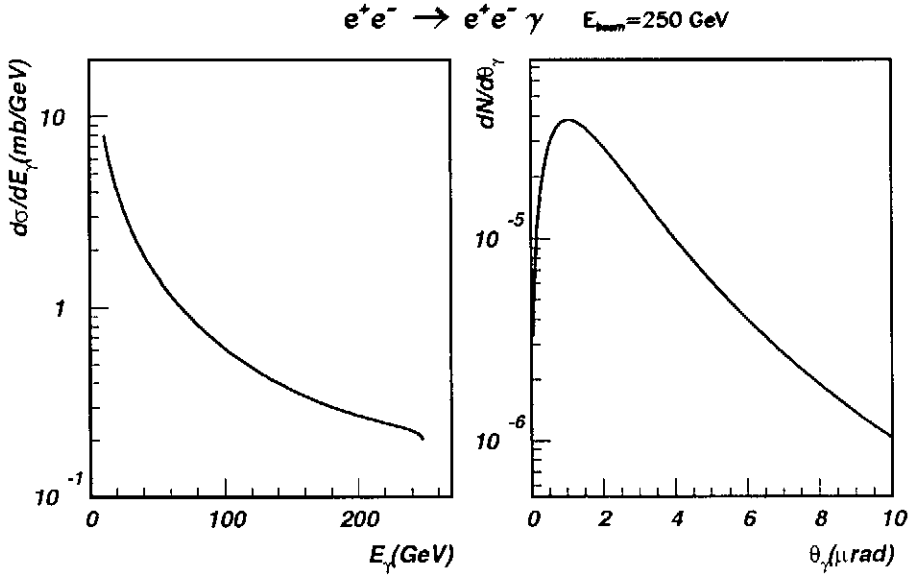

Figure 1: The differential cross-section $d\sigma/dE_\gamma$ and angular distribution of high-energy bremsstrahlung for the colliding 250 GeV e^+e^- beams.

On the other hand, the small transverse momentum transfers correspond to large impact parameters in the e^+e^- collisions and when the lateral beam-size (σ_x, σ_y) is much smaller than the relevant impact parameters $\rho \lesssim \frac{1-y}{y}\frac{E^2_{beam}}{M^3_e}$ then bremsstrahlung is also suppressed. The effect was discovered at VEPP–4 [2] and recently confirmed at HERA [3]. At LEP it explained unexpectedly good beam lifetimes. In the following estimates of this effect at the linear colliders the relevant formulae and useful approximations from the review by Kotkin *et al.* [4] have been used.

It is worth noting that for both effects the suppression decreases with photon energy.

The bremsstrahlung cross-section is sizable even for the highest photon energies and the bremsstrahlung angular distribution is very narrow with a typical angle between the direction of incident electron or positron and that of the radiated photon, θ_γ, of the order of M_e/E_{beam}, see Fig. 1.

If the beam longitudinal polarization P^L_e is non-zero then the bremsstrahlung photons also acquire some degree of circular polarization P^C_γ according to:

$$P^C_\gamma = P^L_e \frac{y(4-y)}{4(1-y)+3y^2}\,.$$

It follows that at $y = 1$ $P^C_\gamma = P^L_e$, and that P^C_γ is near P^L_e if y is close to 1, e.g. if y=0.9 then $P^C_\gamma = 0.986 P^L_e$. The photon polarization is not affected by the bremsstrahlung suppression effects.

In summary, detection of high-energy photons in $e^+e^- \to e^+e^-\gamma$ process at the linear colliders offers a unique opportunity of a direct control of parameters of the beam collisions, i.e.:

- calibration of beam energy from the position of 'end-point' of the bremsstrahlung spectrum, see Fig. 1;
- monitoring beam tilt and angular divergence by measuring photon beam profile;
- absolute luminosity measurement;
- measurement of the longitudinal beam polarization.

3 TESLA case

To consider the proposed method in somewhat more details the TESLA design parameters, $E_{beam} = 250$ GeV, $N = 2 \times 10^{10}$, $\sigma_x = 553$ nm, $\sigma_y = 5$ nm and $\sigma_z = 0.4$ mm, are assumed in the following. For these parameters one obtains $\langle\theta_\gamma\rangle \approx 2$ μrad, $l_f \approx 0.4(1-y)/y$ μm, $\Upsilon \approx 0.04$ and $\rho \lesssim 0.1(1-y)/y$ m.

Since the expected beam divergence is about 40 μrad therefore the produced photons accurately map the angular distribution of beam electrons at the IP.

For y close to 1 (i.e. $y \gg 0.07$) the bremsstrahlung suppression due to the opposite beam charge is small. In contrast, the beam-size effect is significant even at $y = 1$ where it results in about 40% suppression, see Fig. 2. However, the suppression depends only logarithmically on σ_x and σ_y hence, for example, if the beam size is known to 10% the resulting uncertainty of the corrected cross-section is only 1%. It is remarkable that the bremsstrahlung spectrum become much flatter making determination of the ene-point position even more reliable.

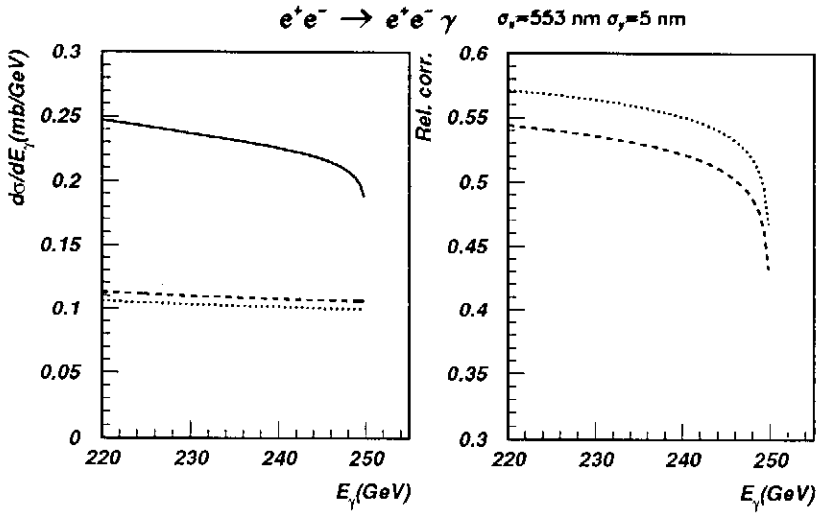

Figure 2: High-energy part of the differential cross-section $d\sigma/dE_\gamma$. Suppression due to the finite beam-size at the IP for the nominal TESLA parameters (dashed lines) and for two times smaller beams (dotted lines).

The angular distributions of the bremsstrahlung is not significantly affected by the beam-size effect as can be seen in Fig. 3.

The detector could be placed some 150 m from the IP where the beams are bent and bremsstrahlung photons can leave the vacuum vessel. The photon beam spot at that location is about 1 cm×1 cm. To select photons with $y \approx 1$

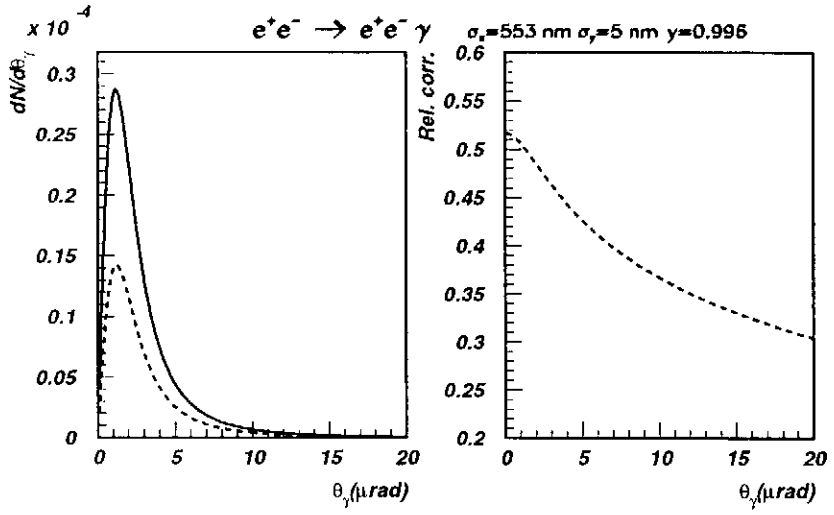

Figure 3: Angular distributions of bremsstrahlung for infinite beams (solid line) and for the suppressed bremsstrahlung at TESLA.

one has to reconstruct single events but on the other hand, the number of high-energy photons produced in one bunch crossing is much larger than one (e.g. for $E_\gamma > 200$ GeV one expects about 4000 events). A possible solution could be to use a thin moving wire or a set of parallel wires to convert only a small fraction of photons into e^+e^- pairs. The electron and positron sharing moreless equally energy of the incident photon could be then analyzed by a dipole magnet and small tracking detectors placed behind the wire target.

Measurement of the rate of $y \approx 1$ photons should potentially provide a precise few per cent luminosity determination. A bunch-to-bunch measurement should also be possible. To match intrinsic angular resolution some 300 μm position reconstruction should be maintained. As was already mentioned, the beam energy calibration could be done and should be limited only by the intrinsic energy scale uncertainty of the e^+e^- analyzer and possible background contamination. The additional smearing of the end-point edge could perhaps be used to estimate the beam energy smearing due to beamstrahlung. The circular polarization of the photons could be measured using coherent effects in thick crystals as proposed by Cabbibo *et al.* [5]. The experimental setup might

be similar to that proposed for HERA [6]. The proof-of-principle experiment to demonstrate feasibility of this experimental technique is underway at CERN [7].

The major remaining issues are the way of integration of such a detector withing the collider beam-line and the level of background events. For the latter, one expects that only high-energy beamstrahlung is relevant. For example, at a half beam energy the rate of beamstrahlung photons is almost hundred times bigger than that for bremsstrahlung. A significant fraction of such beamstrahlung photons would convert into asymmetric e^+e^- pairs. Accidental coincidence of two such events (one with a high-energy e^+ and one with an energetic e^-) would fake a real $y \approx 1$ event. To avoid it either thickness of the target should be very small but then the signal rate would be much less than ≈ 14 kHz rate of beam collisions or, the detector would be very granular and capable of handling many simultaneous events. The accidental background could be then suppressed by imposing tight vertex cuts.

4 Summary

High-energy bremsstrahlung at the future linear colliders seems to offer unique capability of fast and reliable control of major beam parameters at the IP and precise luminosity measurement. Development of a reliable detection method of $y \approx 1$ photons requires further investigations but an attractive solution has been already suggested in this paper for the TESLA layout.

Acknowledgments

Useful comments and discussions with O. Napoly and V. Telnov are gratefully acknowledged.

References

1. P Chen and S Klein in *Advanced Accelerator Concepts*, ed. J S Wurtele (Amer. Inst. Phys., New York, 1993), and references therein.
2. A E Blinov *et al.*, *Phys. Lett.* B **113**, 423 (1982).
3. K Piotrzkowski, *Z. Phys.* C **67**, 577 (1995).
4. G L Kotkin, V G Serbo and A Schiller, *Int. J. Mod. Phys. A* **7**, 4707 (1992).
5. N Cabbibo *et al.*, *Phys. Rev. Lett.* **9**, 270 (1962);
   N Cabbibo *et al.*, *Phys. Rev. Lett.* **9**, 435 (1962).
6. K Piotrzkowski, *Nucl. Instrum. Methods B* **119**, 253 (1996).
7. NA59 Coll., CERN–SPSC–98–17, CERN, July 1998.

GAMMA-GAMMA, GAMMA-ELECTRON COLLIDERS: PHYSICS, LUMINOSITIES, BACKGROUNDS.

V.I. TELNOV
Institute of Nuclear Physics, 630090 Novosibirsk, Russia
email:telnov@inp.nsk.su

This report on Photon Colliders covers the following "physics" issues: physics motivation, possible luminosities, backgrounds, plans of works and international cooperation. More technical aspects such as accelerator issues, new ideas on laser optics, laser cooling, and interaction region layout are discussed in my second talk at this Workshop.

1 Introduction

In addition to e^+e^- collisions, linear colliders provide a unique possibility to study $\gamma\gamma$ and γe interactions at energies and luminosities comparable to those in e^+e^- collisions.[1-6] High energy photons for $\gamma\gamma$, γe collisions can be obtained using laser backscattering. Modern laser technology presents the real possibility for construction of the laser system for $\gamma\gamma$, γe collider ('photon collider'). This option is now included in the pre-conceptual design of the NLC (North American)[7], TESLA (European)[8] and JLC (Asian)[9] linear collider projects in the energy range of a few hundred GeV to about 1.5 TeV. These teams have intent so submit full conceptual design reports in 2001-2002. However, in our time of tight HEP budgets the physics community needs a very clear answer to the following question: a) can $\gamma\gamma$,γe collisions give new physics information in addition to e^+e^- collisions that could justify an additional collider cost (~15%, including detector); b) is it technically feasible; c) is there enough people who are ready to spend a significant part of their career for the design and construction of a photon collider, and exploiting its unique science?

Shortly, my answers are the following:

a) Certainly yes. There are many predictions of extremely interesting physics in the region of the next linear colliders. If something new will be discovered (Higgs, supersymmetry or ... quantum gravity with extra dimensions), to understand better the nature of these new phenomena they should be studied in different reactions which give complementary information.

b) There are no show-stoppers. There are good ideas on obtaining very high luminosities, on laser and optical schemes. It is clear how to remove the disrupted beams and there is an understanding of backgrounds. However, much remains to be done in terms of detailed studies and experimental tests. Special efforts are required for the development of the laser and optics which are the key elements of photon colliders.

c) This is a new direction and it has to pass several natural phases of development. In the last almost two decade, a general conception of photon colliders has been developed and has been discussed at many workshops, the bibliography on $\gamma\gamma$, γe physics now numbers over 1000 papers, mostly theoretical. The next phase will require much wider participation of the experimental community.

To this end, it was recently decided to initiate an International collaboration on Photon Colliders. This Collaboration does not replace the regional working groups, but rather supports and strengthens them. The Invitation letter, signed by Worldwide Study contact persons on photon colliders: V.Telnov (Europe), K. Van Bibber (North America), T.Takahashi (Asia) will be send to you shortly.

2 Physics

2.1 Higgs

The Higgs boson will be produced at photon colliders as a single resonance. This process goes via the loop and its cross section is very sensitive to all heavy (even super-heavy) charged particles which get their mass via the Higgs mechanism. The mass of the Higgs most probably lies in the region of 100< M_H <250 GeV. The effective cross section is presented in Fig. 1.[10]

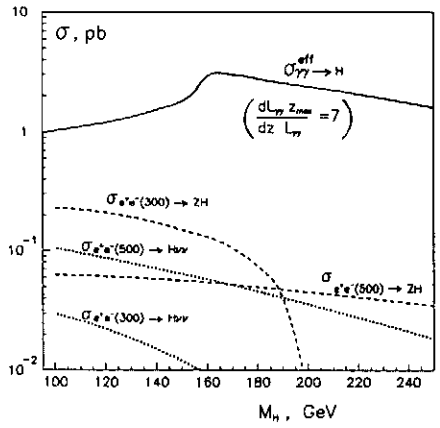

Figure 1: Cross sections for the Standard model Higgs in $\gamma\gamma$ and e^+e^- collisions.

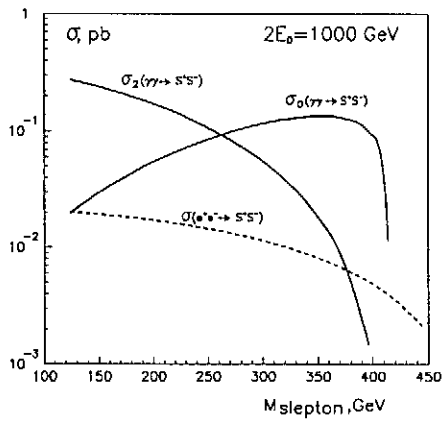

Figure 2: Cross sections for charged scalars production in e^+e^- and $\gamma\gamma$ collisions at $2E_0$ = 1 TeV collider (in $\gamma\gamma$ collision $W_{max} \approx$ 0.82 TeV, $x = 4.6$); σ_0 and σ_2 correspond to the total $\gamma\gamma$ helicity 0 and 2.

Note that here $L_{\gamma\gamma}$ is defined as the $\gamma\gamma$ luminosity at the high energy luminosity peak ($z = W_{\gamma\gamma}/2E_e > 0.65$ for $x = 4.8$) with FWHM about 15%. For comparison, the cross sections of the Higgs production in e^+e^- collisions are shown. We see that for M_H = 120–250 GeV the effective cross section in $\gamma\gamma$ collisions is larger than that in e^+e^- collisions by a factor of about 6–30. If the Higgs is light enough, its width is much less than the energy spread in $\gamma\gamma$ collisions. It can be detected as a peak in the invariant mass distribution or can be searched for by energy scanning using the very sharp ($\sim$ 1%) high energy edge of luminosity distribution.[10] The total number of events in the main decay channels $H \to b\bar{b}, WW(W^*), ZZ(Z^*)$ will be several thousands for a typical integrated luminosity of 10 fb.$^{-1}$ The scanning method also enables the measurement of the Higgs mass with a high precision.

2.2 Charge pair production

The second example is the charged pair production. It could be W^+W^- or $t\bar{t}$ pairs or some new, for instance, supersymmetric particles. Cross sections for the production of charged scalar, lepton, and top pairs in $\gamma\gamma$ collisions are larger than those in e^+e^- collisions by a factor of approximately 5–10; for WW production this factor is even larger, about 10–20. The corresponding graphs can be found elsewhere.[4,8,10]

The cross section of the scalar pair production (sleptons, for example) in collision of polarized photons is shown in Fig.2. One can see that for heavy scalars the cross section in collisions of polarized photons is higher than that in e^+e^- collisions by a factor of 10–20. The cross section near the threshold is very sharp (in e^+e^- it contains a factor β^3) and can be used for measurement of particle masses. Note that for scalar selectrons the cross section in e^+e^- collisions is not described by the curve in Fig.2 due to the existence of an additional exchange diagram (exchange by neutralino). Correspondingly the cross section is not described by pure QED (as it takes place in $\gamma\gamma$). Measurement of cross sections in both e^+e^- and $\gamma\gamma$ channels give, certainly, complementary information.

2.3 Accessible masses

In γe collisions, charged supersymmetric particles with masses higher than those in e^+e^- collisions can be produced (a heavy charged particle plus a light neutral). $\gamma\gamma$ collisions also provide higher accessible masses for particles which are produced as a single resonance in $\gamma\gamma$ collisions (such as the Higgs boson).

2.4 Quantum gravity effects in Extra Dimensions.

This new theory [11] is very interesting though beyond my imagination. It suggests a possible explanation of why gravitation forces are so weak in comparison with electroweak forces. According to this theory the gravitational forces are as strong as electroweak forces at small distances in space with extra dimensions and became weak at large distances due to "compactification" of these extra dimensions. It turns out that this extravagant theory can be tested at linear colliders and according to T.Rizzo [12] ($\gamma\gamma \to WW$) and K.Cheung [13] ($\gamma\gamma \to \gamma\gamma$) photon colliders are sensitive up to a factor of 2 higher quantum gravity mass scale than e^+e^- collisions.

3 Luminosity of photon colliders in current designs.

3.1 0.5–1 TeV colliders

Some results of simulation of $\gamma\gamma$ collisions at TESLA, ILC (converged NLC and JLC) and CLIC are presented below in Table 1. Beam parameters were taken the same as those in e^+e^- collisions with the exception of the horizontal beta function at the IP which is taken (quite conservatively) equal to 2 mm for all cases, that is several times smaller than that in e^+e^- collisions due to the absence of beamstrahlung. The conversion point(CP) is situated at distance $b = \gamma\sigma_y$. It is assumed that electron

beams have 85% longitudinal polarization and laser photons have 100% circular polarization.

Table 1: Parameters of $\gamma\gamma$ colliders based on Tesla(T), ILC(I) and CLIC(C).

	T(500)	I(500)	C(500)	T(800)	I(1000)	C(1000)
no deflection, $b = \gamma\sigma_y$, $x = 4.6$						
$N/10^{10}$	2.	0.95	0.4	1.4	0.95	0.4
σ_z, mm	0.4	0.12	0.05	0.3	0.12	0.05
$f_{rep} \times n_b$, kHz	15	11.4	30.1	13.5	11.4	26.6
$\gamma\epsilon_{x,y}/10^{-6}$,m-rad	10/0.03	5/0.1	1.9/0.1	8/0.01	5/0.1	1.5/0.1
$\beta_{x,y}$,mm at IP	2/0.4	2/0.12	2/0.1	2/0.3	2/0.16	2/0.1
$\sigma_{x,y}$,nm	200/5	140/5	88/4.5	140/2	100/4	55/3.2
b, mm	2.4	2.4	2.2	1.5	4	3.1
$L(geom)$, 10^{33}	48	12	10	75	20	19.5
$L_{\gamma\gamma}(z > 0.65), 10^{33}$	4.5	1.1	1.05	7.2	1.75	1.8
$L_{\gamma e}(z > 0.65), 10^{33}$	6.6	2.6	2.8	8	4.2	4.6
$L_{ee}, 10^{33}$	1.2	1.2	1.6	1.1	1.8	2.3
$\theta_x/\theta_{y,max}$, mrad	5.8/6.5	6.5/6.9	6/7	4.6/5	4.6/5.3	4.6/5.5

We see that $\gamma\gamma$ luminosity in the hard part of the spectrum $L_{\gamma\gamma}(z > 0.65) \sim 0.1L(geom)$, numerically it is about $(1/6)L_{e^+e^-}$. Note, that the coefficient 1/6 is not a fundamental constant. The $\gamma\gamma$ luminosity in these projects is determined only by "geometric" ee-luminosity. With some new low emittance electron sources or with laser cooling of electron beams after the damping ring (or photo-guns) one can get, in principle, $L_{\gamma\gamma}(z > 0.65) > L_{e^+e^-}$. The limitations and technical feasibility are discussed in the next section and my second talk at this workshop.

Beside $\gamma\gamma$ collisions, there is considerable γe luminosity (see table) and it is possible to study γe interactions simultaneously with $\gamma\gamma$ collisions.

The normalized $\gamma\gamma$ luminosity spectra for a 0.5 TeV TESLA are shown in Fig.3(left). The luminosity spectrum is decomposed into two parts, with the total helicity of two photons 0 and 2. We see that in the high energy part of the luminosity spectra photons have a high degree of polarization, which is very important for many experiments. In addition to the high energy peak, there is a factor 5–8 larger low energy luminosity. It is produced by photons after multiple Compton scattering and beamstrahlung photons. Fortunately, these events have a large boost and can be easily distinguished from the central high energy events. In the same Fig.3(left) you can see the same spectrum with an additional "soft" cut on the longitudinal momentum of the produced system which suppresses low energy luminosity to a negligible level.

Fig.3 (right) shows the same spectrum with a stronger cut on the longitudinal momentum. In this case, the spectrum has a nice peak with FWHM about 7.5%. On first sight such cut is somewhat artificial because one can directly select events with high invariant masses. The minimum width of the invariant mass distribution depends only on the detector resolution. However, there is a very important example when one can obtain a "collider resolution" somewhat better than the "detector resolution"; this is the case of only two jets in the event when one can restrict

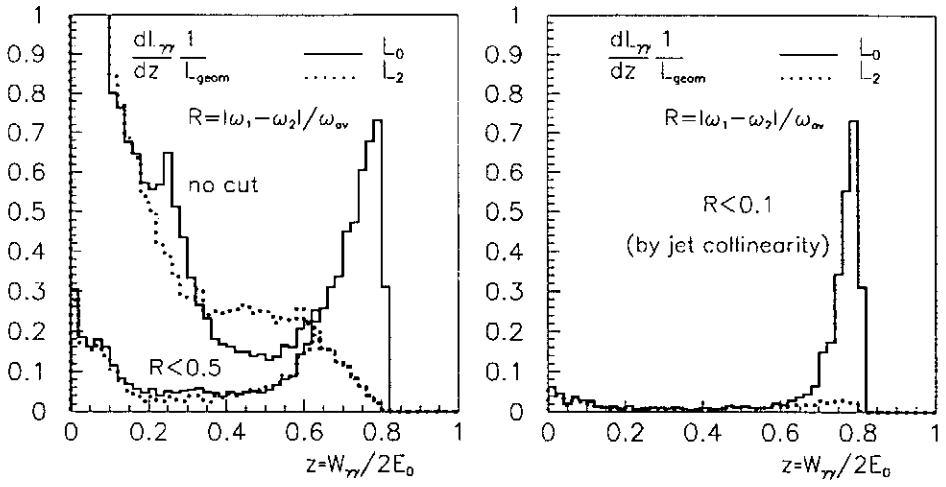

Figure 3: $\gamma\gamma$ luminosity spectra at TESLA(500) for parameters presented in Table 1. Solid line for total helicity of two photons 0 and dotted line for total helicity 2. Upper curves without cuts, two lower pairs of curves have cut on the relative difference of the photon energy. See comments in the text.

the longitudinal momentum of the produced system using the acollinearity angle between jets ($H \to b\bar{b}, \tau\tau$, for example).

A similar table and distributions for the photon collider on the c.m.s. energy 130 GeV (Higgs collider) can be found in ref.[16]

4 Ultimate $\gamma\gamma$, γe luminosities

The $\gamma\gamma$ luminosities in the current projects are determined by the "geometric" luminosity of the electron beams. Having electron beams with smaller emittances one can obtain a much higher $\gamma\gamma$ luminosity.[15] Fig.4 shows dependence of the $\gamma\gamma$ (solid curves) and γe (dashed curves) luminosities on the horizontal beam size. The vertical emittance is taken as in TESLA(500), ILC(500) projects (see Table 1). The horizontal beam size was varied by change of horizontal beam emittance keeping the horizontal beta function at the IP constant and equal to 2 mm.

One can see that all curves for $\gamma\gamma$ luminosity follow their natural behavior: $L \propto 1/\sigma_x$, with the exception of ILC at $2E_0 = 1$ GeV where at small σ_x the effect of coherent pair creation [14,4] is seen.[a] This means that at the same collider the $\gamma\gamma$ luminosity can be increased by decreasing the horizontal beam size at least by one order ($\sigma_x < 10$ nm is difficult due to some effects connected with the crab crossing). Additional increase of $\gamma\gamma$ luminosity by a factor about 3 (TESLA), 7(ILC) can be obtained by a further decrease of the vertical emittance.[16] So, using beams with smaller emittances, the $\gamma\gamma$ luminosity at TELSA, ILC can be increase by almost 2 orders of magnitude. However, even with one order improvement, the number

[a] This curve has also some bend at large σ_x that is connected with synchrotron radiation in quads (Oide effect) due to a large horizontal emittance. One can avoid this effect by taking larger β_x and smaller ϵ_{nx}.

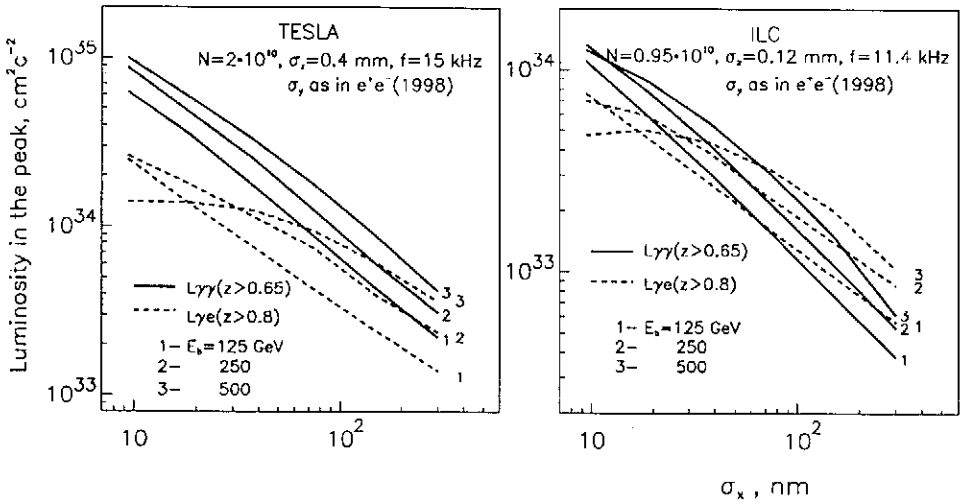

Figure 4: Dependence of $\gamma\gamma$ and γe luminosities in the high energy peak on the horizontal beam size for TESLA and ILC at various energies. See also comments in the text.

of "interesting" events (the Higgs, charged pairs) at photon colliders will be larger than that in e^+e^- collisions by about one order. This is a nice goal and motivation for photon colliders.

In γe collision (Fig.4, dashed curves), the behavior of the luminosity on σ_x is different due to additional collision effects: beams repulsion and beamstrahlung. As a result, the luminosity in the high energy peak is not proportional to the "geometric" luminosity.

There are several ways of decreasing the transverse beam emittances (their product): optimization of storage rings with long wigglers, development of low-emittance RF or pulsed photo-guns with merging many beams with low charge and emittances. Here some progress is certainly possible. Moreover, there is one method which allows further decrease of beam cross sections by two orders in comparison with current designs. It is a laser cooling,[17,18] see my second talk at this workshop.

5 Backgrounds

Sometimes one hears that photon colliders are closer to pp than to e^+e^- colliders because the process $\gamma\gamma \rightarrow hadron$ connected with the hadronic component of the photon, which has a cross section by about 5 orders of magnitude larger than that of electromagnetic production of charged pairs. Continuing this logics line one should say that e^+e^- colliders are, in fact, rather photon colliders than e^+e^- because the cross section of the two-photon process $e^+e^- \rightarrow e^+e^-\ e^+e^-$ is 10–11 orders higher than any of e^+e^- annihilation processes. This is obviously a misleading philosophy.

It is more correct to evaluate the seriousness of background by the problems which it causes for experimentation: recording of data (trigger), their analysis (underlying background processes, overlapping of interesting and background events)

and radiation damage of detector. The proton collider LHC has approximately the same luminosity as a photon collider, but the hadronic background rate is 5 orders magnitude higher; this causes radiation damage of detector components. In this respect photon colliders are much cleaner, practically the same as e^+e^- LC. Nevertheless, the background is a serious issue for both e^+e^- and $\gamma\gamma$ modes at an LC. This is connected mainly with the high luminosity and relatively low beam collision rate that causes many background reactions per each beam collisions.

Let us enumerate the main sources of background at photon colliders:

• *Disrupted beams.* Low energy electrons after the multiple Compton scattering are deflected on opposing electron beam. The maximum disruption angle is about 10 mrad and the energy spread $(0.02-1)E_0$. Solution: all these particles can be removed from the IP using the crab crossing collisions with $\alpha_c \sim 30$ mrad.

• *Electron-positron pairs.* This pairs are produced in the processes $\gamma\gamma \to e^+e^-$, $\gamma e \to e^+e^-$, $ee \to ee + e^+e^-$. There are unavoidable hard large angle particles with acceptable rate and many rather low P_t electrons produced at very small angle and then kicked by the opposing electron beam. Due to solenoidal magnetic field these particles are confined in the region [8]
$r^2[cm^2] < 0.12(N/10^{10})(z[cm]/\sigma_z[mm]B[T])$.
The vacuum pipe should have larger radius. The level of e^+e^- background (mainly in the vertex detector) at photon colliders is is approximately the same as in e^+e^- collisions though some additional study taking into account "reflection" of particles from the mirrors is necessary .

• *Large angle Compton scattering.* The energy of these photon is $\omega = 4\omega_0/\theta^2$ at $\theta \gg 1/\gamma$, where ω_0 is the energy of laser photons ($\sim$ 1 eV). At a distance L the flux of photons $dn/ds \propto N/\gamma^2 L^2 \theta^4$. The main contribution comes from Compton scattering on low energy electrons. The simulation for 2E = 500 GeV gives: $P \sim 10^{-7}$ W/cm^2, $\omega \sim 40$ keV at $\theta = 10$ mrad (the edge of mirrors).

• *Large angle beamstrahlung.* The simulation shows that X-ray photons have a wide spectrum, $P \sim 10^{-6}$ W/cm^2, $\bar{\omega} \sim 1.5$ keV at $\theta = 10$ mrad.

X-rays may cause radiation damage problems for multilayer dielectric mirrors. For our case this problem is not sufficiently studied yet. In principle, there are dielectrical mirrors with very high radiation damage thresholds, sufficient for our task, it should be checked that they have simultaneously high reflectivity. In any case, one can use metal mirrors near the beam, for 1 μm wave length the reflectivity is more than 99 %. Other problems with mirrors: change of the shape due to overheating and carbon deposits due to residual gas. Note, that the X-ray power density on the mirrors is proportional to $1/\vartheta^6$ and, if necessary, the minimum angle can be increased (it is very easy when the mirrors are place outside the beam).

• *Halo of X-rays from final quads.* This is a problem for e^+e^- colliders as well. The solution here is the scraping of electron beam tails by collimators before final focusing. This is not a simple problem, especially if some halo arises after collimation.

• $\gamma\gamma \to$ *hadrons.* Its cross section is $\sigma_{tot} \sim 500$ nb.$^{-1}$ For a typical case $L_{\gamma\gamma} \sim 10^{34}$, $\nu \sim 10^4$ the background rate is 0.5 events/ bunch crossing. Hadronic background was studied in TESLA CDR. [8] It will make problems for certain processes with jets at small angles (such as various QCD processes), however, for the

"main" physics, where products usually have large angles, it should be no serious problem even at maximum expected luminosities (one order higher than at the "nominal" TESLA). It is important to develope algorithms of jet reconstruction which have low sensitivity to "smooth" hadronic background. Influence of hadronic background on quality of reconstruction of various physics processes is one of important tasks of our Study.

6 Conclusion

Prospects of photon colliders for particle physics are great; the physics community should not miss this unique possibility.

1. I.Ginzburg, G.Kotkin, V.Serbo, V.Telnov, *Pizma ZhETF*, **34** (1981) 514; *JETP Lett.* **34** (1982) 491.
2. I.Ginzburg, G.Kotkin, V.Serbo, V.Telnov, *Nucl. Instr. & Meth.* **205** (1983) 47.
3. I.Ginzburg, G.Kotkin, S.Panfil, V.Serbo, V.Telnov, *Nucl. Instr. &Meth.* **219** (1984) 5.
4. V.Telnov, *Nucl. Instr. &Meth.A* **294** (1990) 72; **355** (1995) 3.
5. *Proc.of Workshop on $\gamma\gamma$ Colliders*, Berkeley CA, USA, 1994, *Nucl. Instr. &Meth. A* **355** (1995).
6. A.Sessler, *Gamma ray and muon colliders*, Physics Today, **51** (1998) 48.
7. *Zeroth-Order Design Report for the Next Linear Collider* LBNL-PUB-5424, SLAC Report 474, May 1996.
8. *Conceptual Design of a 500 GeV Electron Positron Linear Collider with Integrated X-Ray Laser Facility* DESY 97-048, ECFA-97-182. R.Brinkmann et al., *Nucl. Instr. &Meth. A* **406** (1998) 13.
9. *JLC Design Study*, KEK-REP-97-1, April 1997. I.Watanabe et. al.,KEK Report 97-17.
10. V.Telnov, *Int. J. Mod. Phys.* A 13 (1998) 2399, e-print:hep-ex/9802003.
11. N. Arkani-Hamed, S. Dimopoulos, G. Dvali. SLAC-PUB-7769, March 1998, Phys. Lett. B 429 (1998) 263, hep-ph/9803315.
12. Thomas Rizzo, SLAC-PUB-8114, April 1999, hep-ex/9904011.
13. Kingman Cheung (UC, Davis). UCD-HEP-99-8, hep-ph/9904266.
14. P.Chen, V.Telnov, *Phys. Rev. Lett.*, **63** (1989) 1796.
15. V.Telnov, *Proc. of ITP Workshop "Future High energy colliders"* Santa Barbara, USA, October 21-25, 1996, AIP Conf. Proc. No 397, p.259-273; e-print: physics/ 9706003.
16. V.Telnov, Proc. of 17th Intern. Conference on High Energy Accelerators (HEACC98), Dubna, Russia, 7-12 Sept. 1998, KEK preprint 98-163, e-print: hep-ex/9810019.
17. V.Telnov, *Phys.Rev.Lett.*, **78** (1997) 4757, erratum ibid 80 (1998) 2747, e-print: hep-ex/9610008.
18. V.Telnov, *Proc. Advanced ICFA Workshop on Quantum aspects of beam physics*, Monterey, USA, 4-9 Jan. 1998, World Scientific, p.173, e-print: hep-ex/9805002.

GAMMA-GAMMA, GAMMA-ELECTRON COLLIDERS: ACCELERATOR, LASER AND INTERACTION REGION ISSUES.

V.I. TELNOV
Institute of Nuclear Physics, 630090 Novosibirsk, Russia
email:telnov@inp.nsk.su

In this report on Photon Colliders the following technical aspects are considered: special requirements to an accelerator, new ideas on laser optics, laser cooling, and interaction region layout issues. In fact it is continuation of my first talk at this workshop where physics motivation, possible luminositics and backgrounds were discussed.

1 Introduction

As a general introduction see my first report from this workshop and references therein.[1] Photon Colliders are based on e^+e^- colliders and the main problem is the same: production of electron beams with low emittances and acceleration to high energies. However, photon colliders have several new features and differences which require special study, especially if we are going to reach ultimate luminosities.[1]

The new key element at photon colliders is a powerful laser system which is used for $e\to\gamma$ conversion. Lasers with required flash energies and pulse duration already exist and are used in several laboratories, the main problem here is the repetition rate. Present technology would already allow the required laser systems to be built now, but it would be very expensive.[2] One very promising way to overcome this problem is discussed in this paper. It is an optical cavity approach, which allows a considerable reduction of the required peak and average laser power.

As you know, in e^+e^- collisions at linear colliders (LC), the beams should be flat in order to restrict the beamstrahlung energy losses. The typical beam sizes at the interaction point (IP) in the current designs are about $\sigma_x/\sigma_y = (300-500)/(3-5)$ nm. Photon colliders with the energies of several hundred GeV can work with practically round beams with a radius of about 1–3 nm. Due to some technical problems connected with the "crab crossing" and the "big bend" and some increase of backgrounds due to a coherent pair creation obtaining and operation with such small horizontal beam sizes at the IP is problematic, but $\sigma_x \sim 10-15$ nm and $\sigma_y \sim 2$ nm is quite a realistic goal.

The main problem in achieving ultimate $\gamma\gamma$ luminosities is the generation of electron beams with very small emittances both in the vertical and horizontal planes. Damping rings can produce, in principle, the required vertical emittance, but the horizontal emittance is larger than desired by two orders of magnitude. Production of such low emittances in both transverse directions is a very challenging task. Now I see only one method to reach this goal, it is laser cooling.[6,7] The required laser system should be much more powerful than that needed for $e\to\gamma$ conversion, but it is not impossible that using the optical cavity scheme such a system can already be built now. The problems in the laser cooling and possible solutions are discussed in sect. 3.

The third group of problems is connected with transportation of low emittance beams to the interaction point, collision and removal of the disrupted beams without generation of additional backgrounds.

2 Lasers, optics

2.1 Requirements for the laser, wave length, flash energy

Laser parameters important for this task are: laser flash energy, duration of laser pulse, wave length and repetition rate. The required wave length follows from the kinematics of Compton scattering.[3] In the conversion region a laser photon with the energy ω_0 scatters at a small collision angle α_0 on a high energy electron with the energy E_0. The maximum energy of scattered photons (in direction of electrons)

$$\omega_m = \frac{x}{x+1}E_0; \quad x = \frac{4E_0\omega_0}{m^2c^4} \simeq 15.3\left[\frac{E_0}{\mathrm{TeV}}\right]\left[\frac{\omega_0}{eV}\right] = 19\left[\frac{E_0}{\mathrm{TeV}}\right]\left[\frac{\mu m}{\lambda}\right].$$

For example: E_0 =250 GeV, ω_0 = 1.17 eV (λ = 1.06 μm) (Nd:Glass laser) $\Rightarrow$ x = 4.5 and ω/E_0 = 0.82. The energy of the backscattered photons grows with increasing x. However, at $x > 4.8$ the high energy photons are lost due to e^+e^- creation in the collisions with laser photons.[4] The maximum conversion coefficient (effective) at $x \sim 10$ is about 0.33 while at $x < 4.8$ it is about 0.65 (one conversion length). The luminosity in the first case will be smaller by a factor of 4. Detailed study of dependence of the maximum $\gamma\gamma$ luminosity and monochromaticity on x can be found elesewhere.[4]

In the laser focus at photon colliders the field is so strong that multiphoton processes can take place, for example, the electron can scatter simultaneously on several laser photons. It is preferable to work in a regime where these effects are small enough, because the shape of the photon spectrum is better. Sometimes strong fields can be useful. Due to transverse motion of electrons in the laser wave the effective electron mass is increased and the threshold of e^+e^- production is shifted to the higher beam energies, a factor of 1.5–2 is possible without special problems "simply" by adding a laser power. For some tasks, such as the energy scanning of the low mass Higgs, the luminosity spectrum should be very sharp, that is only possible when multiphoton effects are small.

From all this it follows that an existing powerful Terawatt solid state laser with the wave length about 1 μm can be used for photon colliders up to c.m.s. energies about 1 TeV. For low energy colliders (for study of the low mass Higgs, for instance), the doubling of the laser frequency may be useful, this can be done with high efficiency, about 45 %.

In the calculation of the required flash energy one has to take into account the natural "diffraction" emittance of the laser beam, the maximum allowed value of the field strength (characterized by the parameter $\xi^2 = (eB\hbar/m\omega_0 c)^2$) and the laser spot size at the conversion point which should be larger than that of the electron beam. In the scheme with crab crossing the electron beam is tilted in respect to the direction of motion that creates an additional effective transverse beam size $\sigma_x = \sigma_z\alpha_c/2$. The result of MC simulation of k^2 (proportional to the $\gamma\gamma$ luminosity)

as a function of the flash energy and parameter ξ^2 (in the center of the laser bunch) are shown in fig. 1 and 2.

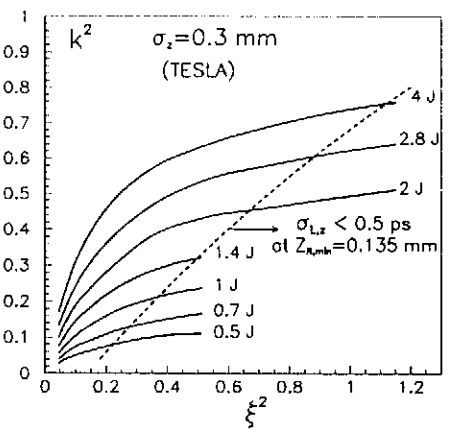

Figure 1: The conversion probability for the various laser flash energies and the values of the parameter ξ^2. Electron beams pass through the holes in the mirrors. See comments in the text.

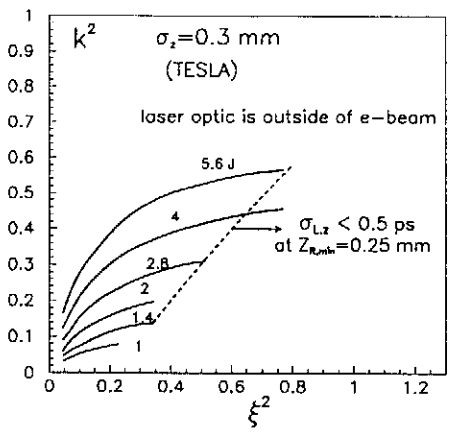

Figure 2: Same as on fig.1, but the mirror system is situated outside the electron beam trajectories.

In summary: the required flash energy is about 3–5 Joules, that is quite reasonable. However, the LC have a repetition rate of about 10-15 kHz, so the average power of the laser system should be up to about 50 kW. [a] One possible scheme is a multi-laser system which combines pulses into one train using Pockels cells. [5] However, such a system will be huge and very expensive. [2]

2.2 Multi-pass laser systems

To overcome the "repetition rate" problem it is quite natural to consider a laser system where one laser bunch is used for e→ γ conversion many times. Indeed, one Joule laser flash contains about 10^{19} laser photons and only 10^{10} photons are knocked out in the collision with one electron bunch.

The simplest solution is to trap the laser pulse to some optical loop and use it many times. [5] In such a system the laser pulse enters via the film polarizer and then is trapped using Pockels cells and polarization rotating plates. Unfortunately, such a system will not work with Terawatt laser pulses due to a self-focusing effect.

Fortunately, there is one way to "create" a powerful laser pulse in the optical "trap" without any material inside. This very promising technique is discussed below.

[a] Though the average power in the one bunch train is higher, the cooling time (namely overheating of the crystals is the main problem) is longer than the time between trains, therefore we can speak about average power.

2.3 Laser pulse stacking in an "external" optical cavity.

Shortly, the method is the following. Using the train of low energy laser pulses one can create in the external passive cavity (with one mirror having some small transparency) an optical pulse of the same duration but with much higher energy (pulse stacking). This pulse circulates many times in the cavity each time colliding with electron bunches passing the center of the cavity.

The idea of pulse stacking is simple but not trivial and not well known in the HEP community (and even to laser experts, though it is as old as the Fabry-Perot interferometer). This method is used now in several experiments on detection of gravitation waves. It was mentioned also in NLC ZDR [5] though without analysis and further development. In my opinion, pulse stacking is very natural for photon colliders and allows not only to build a relatively cheap laser system for $e \to \gamma$ conversion but gives us the practical way for realization of laser cooling, i.e. opens up the way to ultimate luminosities of photon colliders.

As this is very important for photon colliders, let me consider this method in more detail. The principle of pulse stacking is shown in Fig.3. The secret

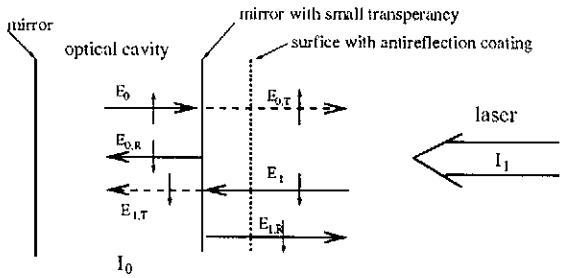

Figure 3: Principle of pulse stacking in an external optical cavity.

consists in the following. There is a well known optical theorem: at any surface, the reflection coefficients for light coming from one and the other sides have opposite signs. In our case, this means that light from the laser entering through semi-transparent mirror into the cavity interferes with reflected light inside the cavity **constructively**, while the light leaking from the cavity interferes with the reflected laser light **destructively**. Namely, this fact produces asymmetry between cavity and space outside the cavity!

Let R be the reflection coefficient, T the transparency coefficient and δ the passive losses in the right mirror. From the energy conservation $R+T+\delta = 1$. Let E_1 and E_0 be the amplitudes of the laser field and the field inside the cavity. In equilibrium, $E_0 = E_{0,R} + E_{1,T}$. Taking into account that $E_{0,R} = E_0\sqrt{R}$, $E_{1,T} = E_1\sqrt{T}$ and $\sqrt{R} \sim 1 - T/2 - \delta/2$ for $R \approx 1$ we obtain $E_0^2/E_1^2 = 4T/(T+\delta)^2$. The maximum ratio of intensities is obtained at $T = \delta$, then $I_0/I_1 = 1/\delta \approx Q$, where Q is the quality factor of the optical cavity. Even with two metal mirrors inside the cavity, one can hope to get a gain factor of about 50–100; with multi-layer mirrors it can reach 10^5. ILC(TESLA) colliders have 120(2800) electron bunches in the train, so the factor 100(1000) would be perfect for our goal, but even the factor of

ten means a drastic reduction of the cost.

Obtaining of high gains requires a very good stabilization of cavity size: $\delta L \sim \lambda/4\pi Q$, laser wave length: $\delta\lambda/\lambda \sim \lambda/4\pi QL$ and distance between the laser and the cavity: $\delta s \sim \lambda/4\pi$. Otherwise, the condition of constructive interference will not be fulfilled. Besides, the frequency spectrum of the laser should coincide with the cavity modes, that is automatically fulfilled when the ratio of the cavity length and that of the laser oscillator is equal to an integer number 1, 2, 3... .

For $\lambda = 1\ \mu m$ and $Q = 100$, the stability of the cavity length should be about 10^{-7} cm. In the LIGO experiment on detection of gravitational waves which uses similar techniques with $L \sim 4$ km and $Q \sim 10^5$ the expected sensitivity is about 10^{-16} cm. In comparison with this project our goal seems to be very realistic.

In HEP literature I have found only one reference on pulse stacking of short pulses ($\sim$ 1 ps) generated by FEL[8] with the wave length of 5 μm. They observed pulses in the cavity with 70 times the energy of the incident FEL pulses, though no long term stabilization was done.

Possible layout of the optics at the interaction region scheme is shown in Fig.4. In this variant, there are two optical cavities (one for each colliding electron beam) placed outside the electron beams. Another possible variant has only one cavity common for both electron beams. In this case, it is also possible to arrange two conversion points separated by the distance of several millimeters (as it is required for photon colliders), though the distribution of the field in the cavity is not completely stable in this case (though it may be sufficient for not too large a Q and , it can be made stable in more complicated optical system). Also, mirrors should have holes for electron beams (which does not change the Q factor of the cavity too much). The previous variant is simpler though it requires a factor of 2 higher flash energy.

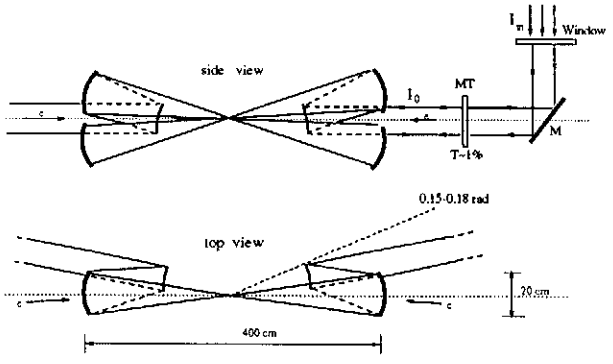

Figure 4: Possible scheme of optics at the IR.

3 Laser cooling of electron beams

The use of pulse stacking in the optical cavity makes the idea of laser cooling[6,7] very realistic, though the required flash energy is one order higher than that required for $e \to \gamma$ conversion. In the method of laser cooling the electron beam at an energy of

about 5 GeV (just after the damping ring and longitudinal compression) is collided 1–2 times with a powerful laser flash losing in each collision a large fraction ($\sim$ 90 %) of its energy to the radiation (Compton scattering), with re-acceleration between cooling sections. The physics of the cooling process is almost the same as radiative cooling of electrons in damping rings. However, here the process takes only 1 ps and the ultimate emittance is much lower than that in the damping rings. This is because in the "linear" laser cooling there are no bends which cause a growth of the horizontal emittance. Also the intra-beam scattering is not important due to a short "damping" time and following fast acceleration. Considering a practical scheme for laser cooling we should take into account many important practical aspects:

• Radiation damage of the mirrors. X-ray radiation due to the Compton scattering here is many orders larger than the radiation level at the same angles in the $\gamma \rightarrow e$ conversion point. It is so because a) the electron energies are lower and b) each electron undergoes about one hundred Compton scattering. At $\vartheta \gg 1/\gamma$ and $x \ll 1$ (x is defined in sect.2) the energy of the Compton scattered photons $\omega = 4\omega_0/\vartheta^2$ and does not depend on the electron energy.[3] However, at the lower beam energies the spectrum is softer ($\omega_{max} = 4\omega_0\gamma^2$) and more photons (per one Compton scattering) have large angles. Simple calculations show that the number of photons/per electron emitted on the angle ϑ during the cooling of electrons from some large energy to the energy E_{min} is

$$dn/d\Omega = mc^2/4\pi\omega_0\gamma_{min}^3\vartheta^4.$$

The total energy hitting the mirrors/cm^2/sec is

$$dP/dS = mc^2 N\nu/\pi\gamma_{min}^3\vartheta^6 L^2,$$

where L is the distance between the collision (cooling) point (CP) and the focusing mirrors, N and ν are the number of electrons in the bunch and the collision rate. One can see a strong dependence of X-ray background on γ_{min} and ϑ. During the cooling the electron beam loses almost all its energy to photons. For $E_0 = 5$ GeV, $N = 2 \times 10^{10}$, $\nu = 15$ kHz the total energy losses are about 200 kW, fortunately the flux decreases rapidly with increasing the angle. At $\vartheta = 30$ mrad and $L = 5$ m the power density $dP/dS \sim 10^{-5}$ W/cm^2 and X-ray photons have an energies of about 4 keV (for 1 μm laser wave length). My estimations shows that rescattering of photons on the quads can give a comparable background.

I have describing this item in detail because for laser cooling the required flash energy is very high and to reach the goal we need very high reflectivity of the mirrors in the optical cavity. For TESLA with 3000 bunches in a train it would be nice to have mirrors with $R > 0.999$. Such values of R are not a problem for dielectric mirrors, however the radiation damage may cause problems, better to avoid this problem.

• Laser spot size should be several times larger than that of the focused electron beam to avoid an additional energy spread of the cooled electrons.

• The cooled electron beam at the energy E=500-1000 GeV has an energy spread of $\sigma_E/E \sim 15$ % at the point where the β- function is small ($\sim 1 - 5$ mm). Matching this beam with the accelerator is not a simple problem and requires special

insertions for chromaticity correction. A similar problem exists for the final focus at linear colliders, it has been solved and tested at the FFTB at SLAC. Here the factor $(F/\beta)\sigma_E/E$ characterizing the chromaticity problem is smaller and the beam energy is 500 times smaller, so one can hope that it will be no problem.

• The parameter ξ^2 (defined above) should be small enough (≤ 1) to keep the minimum attainable emittance, depolarization and the energy spread small enough.[6,7] This is impossible with one laser (with required flash energy) without additional "stretching" of the cooling region along the beam line. The simplest way to do this is to focus several lasers at different points along the beam axis.

The possible optical scheme for the TESLA project is shown in fig.5 (only the final focusing mirrors are shown). The system consist of 8 independent identical

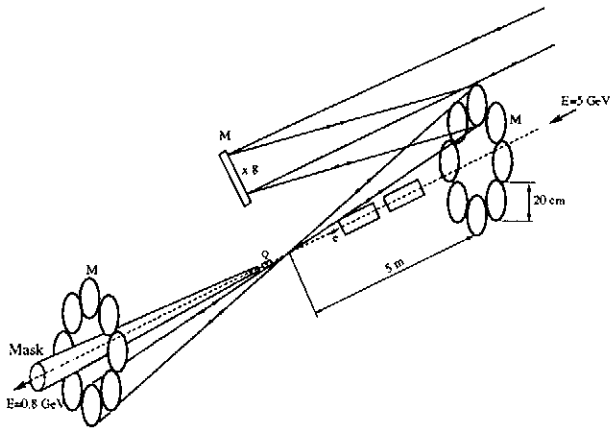

Figure 5: Possible scheme of laser cooling.

optical cavities focusing the laser beams to the points distibuted along the beam direction on the length $\Delta z \sim 2$ mm. The length of the cavity (the distance between the "left" mirror and an entrance semi-transparent mirror (not shown)) is equal to half the distance between the electron bunches in the train, 50 m for TESLA). The large enough angle between the edges of the mirrors and the beam axis (30 mrad) makes X-ray flux rather small (see the estimation above). Also this clear angle allows the final quads to be placed at a distance about 50 cm (from the side of the cooled beam), much closer than the focusing mirrors. Smaller focal distance makes the problem of chromaticity correction easier.

The maximum distance from the CP to the mirrors is determined only by the mirror size, the diameter of 20 cm seems reasonable, which gives $L = 5$ m. The laser spot size at the CP is 7.5 μm, at least 3 times larger than the horizontal electron beam size with $\beta_x < 5$ mm. The circulating flash energy in each cavity is 25 J and 200 J in the whole system, not small. The average power circulating inside the system is 200 × 15 kHz = 3 MW! However, if the Q factor of the cavities is about 1000–3000 (3000 bunches in the electron train at TESLA), the required laser power is only 1–3 kW, or 0.15–0.4 kW/per each laser, that is already reasonable.

What about damage to the mirrors by such powerful laser light? The maximum

laser flash energy/cm^2 on the mirrors is 0.13 J/cm^2 (0.7-2 has been achieved for 1 ps pulses [5]), the average power/cm^2 is 2 kW/cm^2 (there are systems with > 5 kW/cm^2 working long time [5]). The average power inside one train ($\Delta t = 1$ msec) is 200 times higher (400 J/1 msec), but from the same ref.[5] is known that 100 J for a time of 100 ns is OK, and extrapolating as $\sqrt{t}$ (thermoconductivity) one can expect the limit of about 10 kJ for 1 msec, much larger that expected in our case. Note, here we are speaking about circulating, not absorbed energy. So, all power densities are below the known limits, this all depends, of course, on specific choice of mirrors.

At last, the main numbers. After one stage of such a cooling system the normalized emittance is decreased by a factor of 6. The ultimate normalized emittance (after several cooling sections) is proportional to the β-function at the CP, at $\beta_{x,y} = 1$ mm it is about 2×10^{-9} m rad, smaller than can be produced by the TESLA damping ring by a factor of 5000(15) in x(y) directions. From this point of view such a small β_x is not necessary, but it should be small enough (< 5 mm to have a small electron spot size in the cooling region. The first stage of cooling will be the most efficient because the beam is cooled in both horizontal and vertical directions (far from the limits). Besides after decreasing the horizontal emittance the β- function at the LC final focus can be made as small as possible, $\sim \sigma_z$. All together this can give a factor of ten in the luminosity.

Having no space for discussion of accelerator aspects in this paper I would like to note only that all systems of the LC should allow beam emittances to be reached which are lower than are necessary for e^+e^- collisions (see the intoduction). Many technical decisions should be done before the beginning of construction works.

4 Conclusion

Photon colliders is a very inspiring new field of high energy physics and I invite you to take part in this venture.

1. V.Telnov, Talk at Intern. Workshop on Physics and experiments at Linear Colliders, Sitges, Spain, April 28, 1998.
2. K. van Bibber, M.Perry, ibid.
3. I.Ginzburg, G.Kotkin, V.Serbo, V.Telnov, *Nucl.Instr.& Meth.* **205** (1983) 47.
4. V.Telnov, *Nucl. Instr. &Meth.A* **294** (1990) 72; *Nucl. Instr. &Meth.A* **355** (1995) 3.
5. *Zeroth-Order Design Report for the Next Linear Collider* LBNL-PUB-5424, SLAC Report 474, May 1996.
6. V.Telnov, *Phys.Rev.Lett.*, **78** (1997) 4757, erratum ibid 80 (1998) 2747, e-print: hep-ex/9610008.
7. V.Telnov, *Proc. Advanced ICFA Workshop on Quantum aspects of beam physics*, Monterey, USA, 4-9 Jan. 1998, World Scientific, p.173, e-print: hep-ex/9805002.
8. T.Smith, P.Haar, H.Schwettman, *Nucl. Instr. &Meth. A* **393** (1997) 245 .